BBA - Molecular Cell Research 1865 (2018) 480–495

Contents lists available at ScienceDirect

BBA - Molecular Cell Research

journal homepage: www.elsevier.com/locate/bbamcr

PUMA dependent mitophagy by *Abrus* agglutinin contributes to apoptosis through ceramide generation

Prashanta Kumar Panda[a], Prajna Paramita Naik[a], Biswa Ranjan Meher[b], Durgesh Nandini Das[a], Subhadip Mukhopadhyay[a], Prakash Priyadarshi Praharaj[a], Tapas K. Maiti[c], Sujit K. Bhutia[a,*]

[a] Department of Life Science, National Institute of Technology, Rourkela, India
[b] Centre for Life Sciences, Central University of Jharkhand, Brambe, Ranchi, Jharkhand, India
[c] Department of Biotechnology, Indian Institute of Technology, Kharagpur, India

ARTICLE INFO

Keywords:
Abrus agglutinin
Mitophagy
Ceramide
PUMA
LC3 interacting region
p62
Ubiquitin
Apoptosis

ABSTRACT

PUMA, a BH3-only pro-apoptotic Bcl2 family protein, is known to translocate from the cytosol into the mitochondria in order to induce apoptosis. Interestingly, the induction of PUMA by p53 plays a critical role in DNA damage-induced apoptosis. In this study, we reported mitophagy inducing potential of PUMA triggered by phytolectin *Abrus* agglutinin (AGG) in U87MG glioblastoma cells and established AGG-induced ceramide acts as the chief mediator of mitophagy dependent cell death through activation of both mitochondrial ROS as well as ER stress. Importantly, AGG upregulates PUMA expression in U87MG cells with the generation of dysfunctional mitochondria, with gain and loss of function of PUMA is shown to alter mitophagy induction. At the molecular level, our study identified that the LC3 interacting region (LIR) located at the C-terminal end of PUMA interacts with LC3 in order to stimulate mitophagy. In addition, AGG is also found to trigger ubiquitination of PUMA which in turn interacted with p62 for prompting mitophagy suggesting that AGG turns on PUMA-mediated mitophagy in U87MG cells in both p62-dependent as well as in p62-independent manner. Interestingly, AGG-triggered ceramide production through activation of ceramide synthase–1 leads to induction of ER stress and ROS accumulation to promote mitochondrial damage as well as mitophagy. Further, upon pre-treatment with Mdivi–1, DRP1 inhibitor, AGG exposure results in suppression of apoptosis in U87MG cells indicating AGG-induced mitophagy switches to apoptosis that can be exploited for better cancer therapeutics.

1. Introduction

The selective clearance of damaged and superfluous mitochondria often referred to as “mitophagy”, is an important phenomenon in many normal developmental and pathophysiological conditions [1–4]. In terms of maintaining cellular homeostasis, mitophagy is a central regulator of both energy balance as well as mitochondrial quality control. It is well established that mitophagy plays an indispensable role in paternal mitochondrial degradation [5], terminal differentiation of RBCs [6], ischemia, neurodegenerative diseases [2,3], cancer [7] and/or drug-induced tissue injury [8]. The process of mitophagy involves priming mitochondria and recruiting them to the autophagosome for specific degradation. Prior to the lysosomal degradation, the depolarized ubiquitinated mitochondria are recruited to the ubiquitin-binding adaptor protein p62/SQSTRM1 located in the perinuclear region so as to form aggregates known as mitoaggresomes [1,8]. Under stressful conditions, PINK1 stabilizes on damaged mitochondria, which results in the recruitment of an E3 ubiquitin ligase (Parkin) that ubiquitinates several outer mitochondrial proteins. This is followed by the recruitment of adaptor proteins such as p62/SQSTM1 which in turn interacts with the LC3 protein to induce mitophagy. Several proteins interact with the autophagosomal marker protein LC3 through a specific LC3-interacting region (LIR) motif. This specific motif acts as a mitophagy receptor in directing mitochondria to autophagosomes. Proteins known to contain this motif include FUNDC1, BNIP3, Nix, VDAC1, PINK1, BCL2L13, and Prohibitin2 [6,9–13]. The core consensus sequence of the LIR motif that is crucial for mitophagy has been identified as W/F/Y-x-x-L/I/V [1,3].

PUMA, a BH3 only proapoptotic protein, plays an important role in the apoptotic pathway. It is known that PUMA exerts its effect through activation of Bax/Bak during situations involving oxidative stress, DNA damage, hypoxia, and growth factor deprivation [14,15]. PUMA can act as an activator as well as an enabler for the apoptotic death of the cell. It can directly activate the pro-apoptotic proteins Bax and Bak through

* Corresponding author at: Department of Life Science, National Institute of Technology Rourkela, Rourkela 769008, Odisha, India.
E-mail address: sujitb@nitrkl.ac.in (S.K. Bhutia).

https://doi.org/10.1016/j.bbamcr.2017.12.002
Received 31 May 2017; Received in revised form 15 November 2017; Accepted 7 December 2017
Available online 08 December 2017

the BH3 domain in order to induce mitochondrial dysfunction. Alternatively, it can indirectly release Bax and Bak by interacting with antiapoptotic Bcl–2 family proteins like Bcl-xL and Bcl–2 and thereby modulate apoptosis [16]. Previously, PUMA was reported to induce autophagy that leads to the selective removal of mitochondria to contribute apoptosis [17]. It elucidated that the autophagic activity of PUMA was mediated through the association of its BH3 domain with Bax or Bak, but the exact mechanism underlying mitochondrial autophagy by PUMA remains unclear.

In the present study, we have investigated glioma inhibitory activity of *Abrus* agglutinin (AGG), a heterotetrameric Type II Ribosome-inactivating protein with galactose specific domain [18] from Indian medical plant through the induction of mitophagy mediated cell death. AGG induces both extrinsic as well as intrinsic apoptosis and exhibits antitumor activity at sub-lethal doses in several tumor models [19–23]. Interestingly, AGG affects apoptosis in cancer by modulating key signaling pathways involving the Bcl–2 family, the caspase family, p73, p38, PI3K/Akt, NF-kB and ERK [20,22–25]. Moreover, AGG inhibits expression of the pro-angiogenic factor IGFBP–2 in an Akt-dependent manner and causes a reduction in the angiogenic phenotype both *in vitro* as well as *in vivo* [22]. Recently, our study has shown that AGG-mediated Akt dephosphorylation leads to ER stress which in turn causes the induction of autophagy-dependent cell death through the canonical pathway in cervical cancer [26]. In this study, we have identified mitophagy-inducing potential of PUMA triggered by AGG in glioblastoma cells and established AGG-induced ceramide as a chief mediator of mitophagy dependent cell death *via* the activation of mitochondrial ROS and ER stress.

2. Materials and methods

2.1. Reagents and chemicals

3-(4,5-Dimethylthiazol-2-yl)-2,5-diphenyltetrazolium (MTT) (M5655), 4′,6-diamidino-2-phenylindole dihydrochloride (DAPI) (D9542), dimethylsulfoxide (DMSO) (D2650), propidium iodide (PI) (P4170), *N*-acetyl-L-cysteine (NAC) (A9615), 3-Methyl adenine (3-MA) (M9281), Salubrinal (324895), Chloroquine (CQ) (C6628), Myriocin (M1177), Methyl pyruvate (371173), Mdivi–1 (M0199) and dihydroethidium (DHE) (D7008) were purchased from Sigma-Aldrich (St Louis, MO, USA). Fetal bovine serum (sterile-filtered, South American origin), Minimal Essential Medium (MEM), opti-MEM, lipofectamine 2000, MitoTracker Green (M7514) and CMxROS (M7512) were purchased from Invitrogen; Caspase 3/7 Glo assay kit (T8090), Caspase 8 Glo assay kit (G8200) and Caspase 9 Glo assay kit (G8210) were purchased from Promega (Madison, Wisconsin, USA).

2.2. Purification of AGG

The purification of AGG was carried out according to the previously reported method [27]. The crude extract of *Abrus precatorius* seed kernels was subjected to 30–90% ammonium sulfate precipitation. This was followed by affinity chromatography using a lactamyl Sephadex-G-100 affinity column. Purified AGG was obtained after subjecting affinity eluted lectins to Sephadex-G-100 gel permeation chromatography using an FPLC system. Lectin activity of AGG was analyzed by the hemagglutination assay and purity of AGG was checked by both SDS as well as native PAGE.

2.3. Antibodies

Antibodies used in this study are as follows: Ceramide (C8104) was obtained from Sigma-Aldrich, St Louis, MO, USA; PUMA (4976S), Beclin–1 (3738S), ATG5-ATG12 (2630S), Bax (2772S), Bcl–2 (2870S), COX IV (4850), pDRP1 (3455), PARP (9542S), p53 (2527BC) were purchased from Cell Signaling Technology (Danvers, MA, USA). LC3B (NB100-2220) was obtained from Novus Biological (Littleton, CO, USA). Mouse secondary Alexa Flour green, mouse secondary Alexa Flour red, rabbit secondary Alexa Flour green and rabbit secondary Alexa Flour red were purchased from Invitrogen (Carlsbad, CA, USA). p62, TOM20, and GRP78 were purchased from BD Bioscience (Franklin Lakes, NJ, USA). γH2AX was purchased from Millipore (Billerica, MA, USA) and actin (11-13012) and LAMP1 (10-7589) were purchased from Abgenex (Bhubaneswar, OD, India). Parkin (PRK8) (sc-32282) was obtained from Santa Cruz Biotechnology (Dallas, TX, USA).

2.4. Plasmid and siRNA

U87MG cells were transiently transfected with pEX-HcRed-hLC3WT (Addgene plasmid #24991) and pEX- HcRed-hLC3ΔG (Addgene plasmid #24992); both the constructs were gifted from Isei Tanida (Addgene plasmid #24991). Additionally, glioblstoma cells were also transfected with pBABEpuro-HA-p62-LIR (gifted by Jayanta Debnath) (Addgene plasmid #71306). For autophagosome clustering study, P(40) PX-EGFP plasmid was transfected in glioma cells (gifted by Michael Yaffe) (Addgene plasmid #19010). The overexpression of PUMA was performed by transfecting pBI-EGFP-PUMA (gifted by Bert Vogelstein) (Addgene plasmid #16590). For further mitophagy study, we expressedmKeima-Red-Mito-7 which was a gift from Michael Davidson (Addgene plasmid#56018). Similarly Parkin overexpression was performed using pEGFP-parkin WTgifted by Edward Fon (Addgene plasmid #45875). A corresponding empty backbone vector was transfected for every plasmid of interest. siRNA for Beclin–1 (sc29797), PUMA (sc-37153), Parkin (sc-42158) and their corresponding sicontrol were obtained from SantaCruz Biotechnology (Dallas, TX, USA).

2.5. Cell culture

Human glioblastoma cell line (U87MG) was obtained from National Centre for Cell Sciences (NCCS), Pune, India and cultured in Minimal Essential Medium (MEM) containing 10% fetal bovine serum (FBS) with 1 × antibiotic-antimycotic and incubated at 37 °C temperature in a humidified 95% air, 5% CO2 incubator.

2.6. Electron microscopy

For transmission electron microscopy (TEM), U87MG cells were rinsed with 0.1 M Sorensen's buffer (pH 7.5), fixed in 2.5% glutaraldehyde for 2 h, and subsequently dehydrated and embedded in Spurr's resin. The block was then sectioned into ultrathin sections and picked up on copper grids. The ultrathin sections were stained with 2% uranyl acetate and lead citrate. Electron micrographs were obtained using a transmission electron microscope (Joel JEM-1230 equipped with a Gatan UltraScan 4000SP 4 K × 4 K CCD camera) [26].

2.7. Immunofluorescence staining and colocalization study

After treatment with AGG, U87MG cells were fixed in 10% formaldehyde followed by washing with PBS. The cells were permeabilized by addition of 0.2% Triton X–100 for 20 min at room temperature followed by overnight (14–16 h) incubation with primary antibody. The cells were then washed with PBS and incubated with secondary antibody for 6 h followed by DAPI counterstaining. The expression pattern of concerned proteins and co-localization studies were conducted using a confocal laser scanning microscope (Leica TCS SP8) [4,26].

2.8. Western blot and immunoprecipitation analysis

U87MG cells were treated with AGG followed by protein extraction. The cells were lysed using a lysis buffer and about 50 μg protein was subjected to SDS-PAGE. This was then followed by transfer onto a nitrocellulose membrane and blocking with 5% BSA (in PBST) at room

temperature for 1 h. Subsequently, the blots were incubated with primary antibody for Beclin-1, ATG5, LC3, actin, p-AMPK, p-S6K, p-mTOR, TOM20, COX-IV, DRP1, p-DRP1, PARP, Bax, Bcl2 and GRP78 for 14–16 h followed by secondary antibody labeled with horseradish peroxidase-conjugated secondary antibody. The expression was documented using chemiluminescence Image Quant LAS500 (GE Healthcare, USA). For immunoprecipitation, cell lysates were incubated overnight at 4 °C with their respective antibodies followed by coupling with protein A-agarose. This was followed by Western blot analysis with a suitable antibody [4].

2.9. Analysis of dysfunctional mitochondria

Mitochondrial mass was measured by analyzing fluorescence levels after staining the cells with 100 nM MitoTrackerGreen FM and MitoTracker Red CMXRos (Molecular Probes/Invitrogen) for 25 min at 37 °C. After staining, the cells were then washed with PBS followed by trypsinization and resuspension in PBS containing 1% fetal bovine serum (FBS) for fluorescence-activated cell sorting (FACS) analysis [4].

2.10. Cell viability assay

U87MG cells were harvested and 1×10^4 cells/well were cultured in a 96-well plate at 37 °C with varying concentrations of AGG for 48 h. A 3-(4,5-dimethylthiazol-2-yl)-2,5-diphenyltetrazolium bromide (MTT) solution (5 mg/ml) was then added to the cells and incubated for 4 h. The resultant formazan crystals were dissolved in dimethyl sulfoxide and the absorbance was measured at 595 nm using a microplate reader (PerkinElmer, Waltham, MA, USA) [22].

2.11. Caspase activity assays

After treatment, caspase 3/7, caspase 8 and caspase 9 activities of the U87MG cells were measured using Caspase-Glo 3/7, Caspase-Glo 8 and Caspase-Glo 9 Assay kits as per the manufacturer's protocol. Caspase activity was analyzed and quantified in terms of relative luciferase units.

2.12. Measurement of mitochondrial respiration rate and glycolysis study

For determining oxygen consumption rate (OCR), 1×10^5 cells/well were seeded in a 96 well plate. The OCR measurement was done using an XF–24 extracellular flux analyzer (Seahorse Bioscience, MA, USA) as per previously reported protocol [4]. The rate of aerobic glycolysis, in terms of enzymatic lactate production, was determined after cells had been exposed to AGG treatment for different time intervals.

2.13. Measurement of cellular ATP level

Cellular ATP content was quantified in U87MG cell lysates 24 h after AGG treatment using the protocol prescribed by the ENLITEN® ATP Assay System Bioluminescence kit procured from Promega (Madison, WI, USA).

2.14. Modeling PUMA-LC3 complex through docking and molecular dynamics simulation

Due to unavailability of hPUMA crystal structure, the 3D structure of the same was predicted by *ab initio* modeling in the PHYRE–2 software using the FASTA sequence of the protein [28]. By the Chou-Fasman method, hPUMA sequence from 128 to 165 aa (AA128-AA165) is described as an alpha-helix [29]. The crystal structure of microtubule-associated protein light chain 3 (LC3), a mammalian homolog of *Saccharomyces cerevisiae* Atg8, was obtained from the Protein Data Bank (PDB) (PDB entry is 1UGM). The X-ray structure of the LC3 domain contains some missing residues in the C– and N-terminal regions, which were eventually predicted by the PHYRE–2 software. After PHYRE–2 modeling, it was seen that the LC3 domain contained 119 residues. A docking algorithm was then used to locate the optimal configuration for the LC3 protein near the active site of hPUMA. Initially, the LC3 domain was positioned near the active site and the docking algorithm was carried out by the ClusPro 2.0 protein-protein docking server. Using protein-protein docking algorithms, the optimal orientation of two proteins was found by scoring the energy based on the van der Waals (VDW) contacts and corresponding electrostatics. Therefore, a grid-based score was generated by calculating the nonbonded terms of the molecular mechanical force field, and the structure with the highest score was then considered for the MD simulation [26].

2.15. Mass spectrometric analysis of ceramides and dihydroceramide species

AGG treated U87MG cells were washed extensively with PBS and detached from the substratum by trypsinization. For ceramide analysis, internal standards were added, lipids were extracted, and individual ceramide acyl chain species were quantified by liquid chromatography and electrospray ionization tandem mass spectrometry as described previously. Ceramide concentrations were expressed as pmole/million cells [30].

2.16. Statistical analysis

All data are representative of at least five independent sets of the experiments, which were quantified and plotted in terms of mean ± standard deviation. Student's *t*-test was used for evaluating statistical differences between experimental groups. Non-parametric tests for statistical analysis between groups were done using the one-way ANOVA Kruskal-Wallis test and with the Dunn's multiple group comparison test wherever appropriate. Statistical analyses were done using the SPSS Statistics 20 (IBM SPSS software, version: 20.0, Chicago, IL, USA) and GraphPad Prism 5 (GraphPad Software, Inc., San Diego, CA, USA). The P-value was defined as follows: non-significant (n.s.): $P > 0.05$; and *: $P < 0.05$; **: $P < 0.01$ were considered as statistically significant.

3. Results

3.1. AGG induces mitochondrial autophagy

Mitophagy refers to the selective autophagosome-mediated mitochondrial degradation process in which damaged and dysfunctional mitochondria are cleared for the maintenance of cellular homeostasis [2,4]. Our previous study showed that AGG induces autophagy-dependent cell death in cervical carcinoma. Here, we established that in glioblastoma cells, AGG induces mitophagy-dependent cell death through activation of both mitochondrial ROS as well as ER stress. After establishing autophagic and apoptotic inducing activity of AGG (Supplementary Figs. S1–S3), U87MG cells were treated with AGG and ultrastructure analysis of the double membrane autophagosome containing mitochondria formation was analyzed by electron microscopy. Electron micrograph showed that mitochondria were specifically affected in AGG treated U87MG cells as compared to control (Fig. 1a and b). The healthy mitochondria could be recognized and quantified by identifying intact cristae; the prevalence of intact mitochondria was determined to be 60 ± 5.9% and 4 ± 0.43% in control and treated group, respectively. The percentage of fragmented mitochondria was computed by counting the number of mitochondria with dramatically disrupted cristae and found to be 28 ± 2.7% and 50 ± 5.1% in control and AGG treated U87MG cells, respectively. Interestingly, we also identified double-membrane autophagosome engulfed damaged mitochondria or mitophagosomes in AGG treated cells. Some of the depolarized fragmented swollen mitochondria, more appropriately

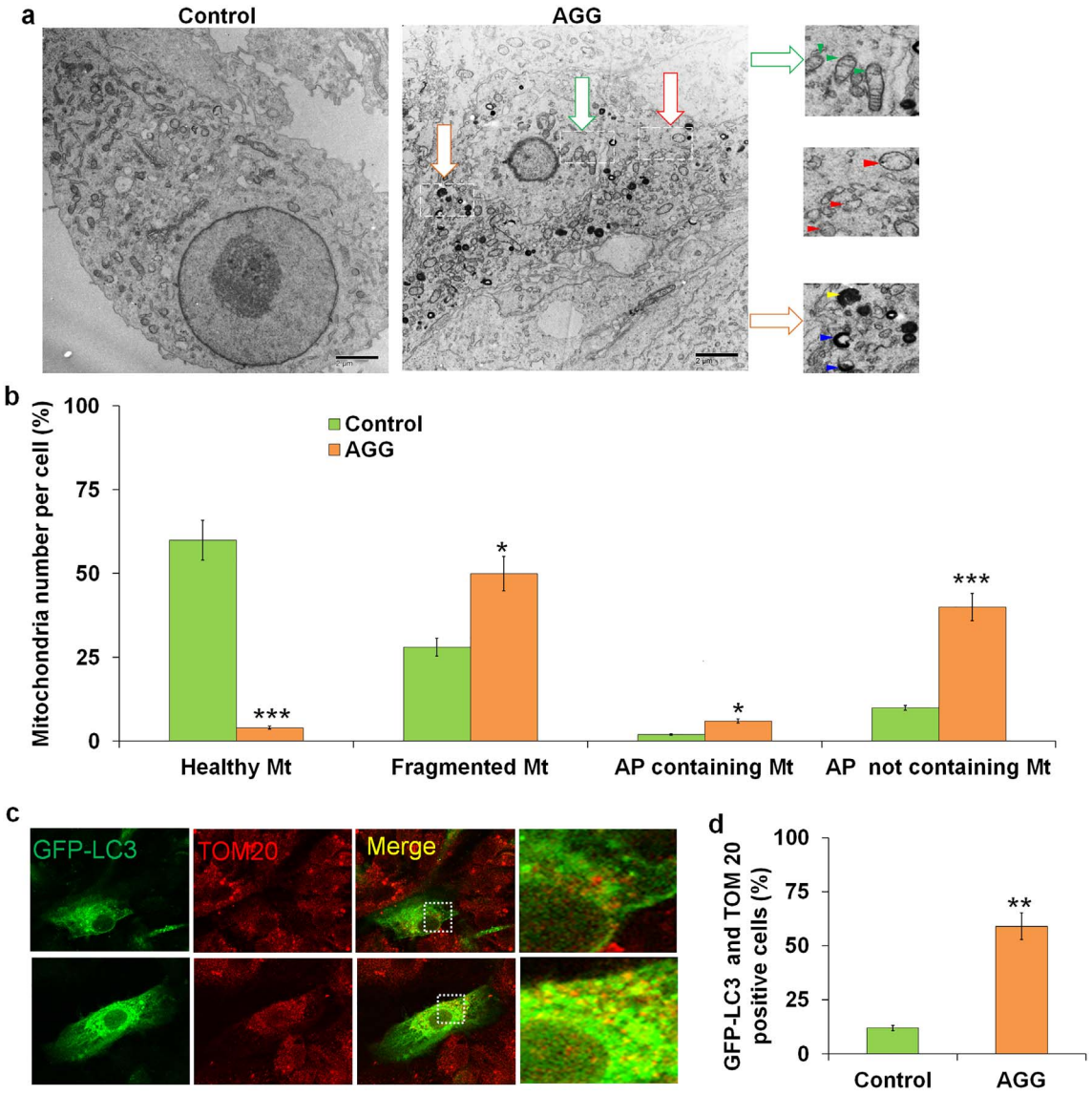

Fig. 1. Effect of AGG on mitochondria in U87MG cells. U87MG cells were treated with AGG for 24 h and the cells were fixed and processed for electron microscopy (a, b). The number of healthy (green arrow), fragmented (red arrow), autophagosome (AP) containing mitochondria (Mt) (yellow arrow) and AP not containing Mt (blue arrow) were quantified. U87MG cells were transfected with GFP-LC3 and stained with TOM20 after 24 h AGG treatment and interaction of LC3 and TOM20 were analyzed through confocal microscopy (c, d). The data reported as the mean ± S.D. of three independent experiments and compared to PBS control. *P-value < 0.05; **P-value < 0.01 and ***P-value < 0.001 were considered significant.

classified as mitochondrial remnants, were observed to be engulfed by the autophagosome. The percentage of this occurrence in control and in AGG treated cells was 2 ± 0.21% and 6 ± 0.61%, respectively. In addition, a significant increase in the number of autophagosome in AGG treated cells (40 ± 4.1%) in comparison to control (10 ± 0.7%) was also observed (Fig. 1b). Immunostaining for the mitochondrial membrane protein TOM20 was used to study mitochondrial degradation through autophagy in GFP-LC3 transfected U87MG cells. Our data showed that an exposure to AGG significantly increased the number of GFP-LC3 and TOM20 positive cells as compared to control suggesting AGG facilitates recognition of mitochondria by the autophagy machinery (Fig. 1c–d). The downregulation of the outer mitochondrial membrane protein TOM20 is generally associated with the clearance of mitochondria *via* mitophagy. Both Western blot and immunofluorescence analysis revealed that U87MG cells showed a dose and time dependent decrease of TOM20 expression upon exposure to AGG for 24 h (Fig. 2a–e). We also quantified the reduction of the integral inner mitochondrial membrane protein cytochrome *c* oxidase subunit 4 (COX IV) after AGG treatment (Fig. 2e). Dynamin-related protein 1 (DRP1) is generally known as the master regulator of the mitochondrial fission process. AGG treatment showed dephosphorylation of DRP1 at its conserved Ser637 residue [3,31] and resulted in the development of depolarized mitochondria as well as in the induction of mitophagy (Fig. 2f). Further, AGG-induced mitophagy was quantified in Beclin–1 knockdown cells (Supplementary Fig. S4a) and in presence of autophagy inhibitors in U87MG cells. Our data showed that as compared to sicontrol, AGG significantly restored the TOM20 expression in Beclin-1 deficient cells (Fig. 2g, h). Similarly, it was observed that in U87MG cells, the expression of COXIV was dramatically reinstated in siBeclin–1 knock downs cells in the presence of AGG as compared to sicontrol (Fig. 2i). The pretreatment with pharmacological inhibitors such as 3-MA and CQ inhibited AGG-induced decrease in expression of TOM20 in U87MG cells (Fig. 2j-m). Next we studied whether mitophagosomes get fused with lysosomes for mitochondrial degradation. We examined mitophagy flux by using mitochondria-targeted mKeima-Red-Mito7, a lysosomal hydrolase resistant probe in which fluorescence changes from green to red in acidic pH as an illustrative of the delivery mitophagosome into the maturing lysosome. As expected, a considerable

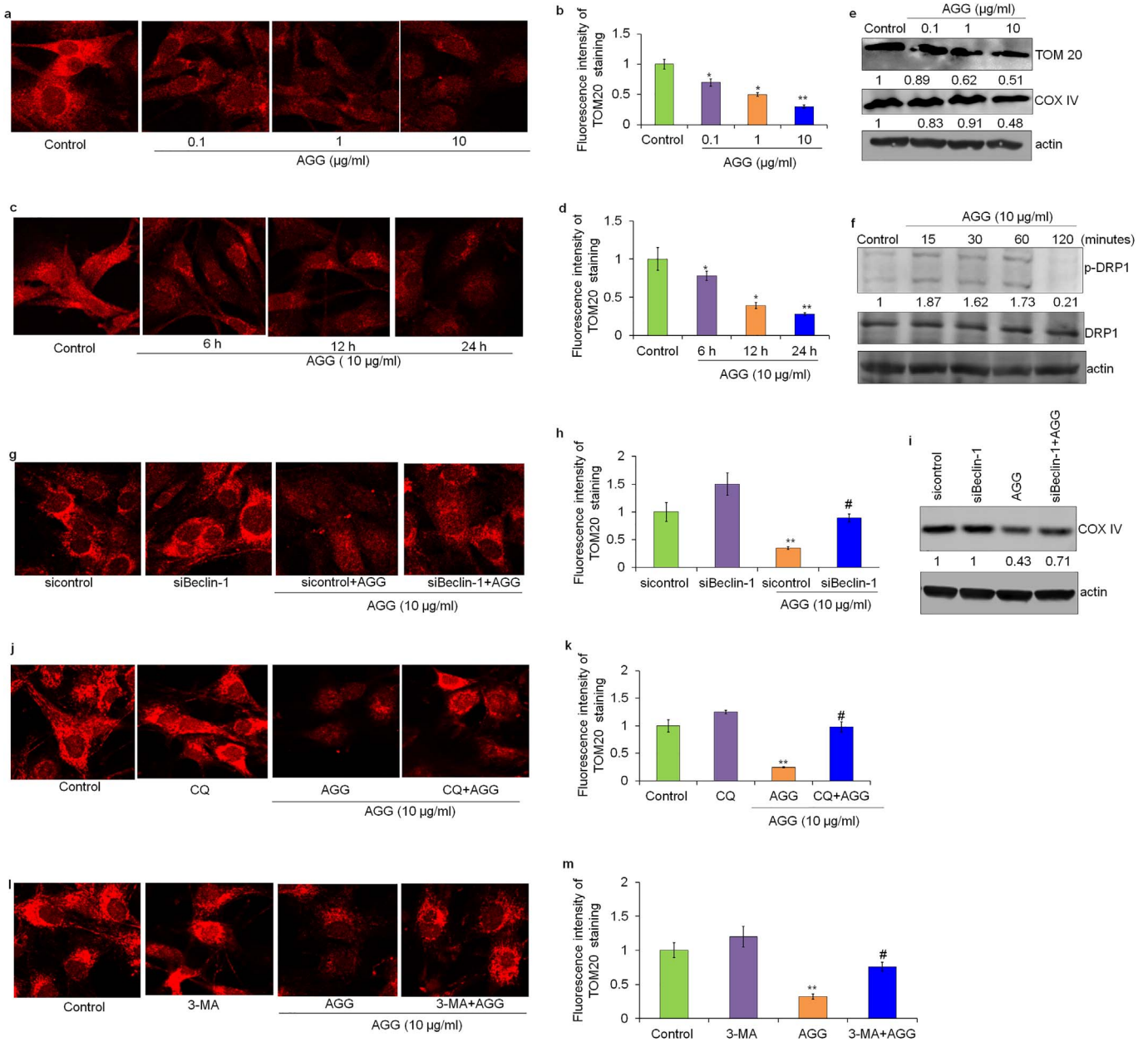

Fig. 2. AGG induces mitochondrial autophagy in U87MG cells. U87MG cells were treated with AGG, the expression of TOM20 was analyzed through confocal microscopy (a–d) and expression of TOM20, COXIV, p-DRP1, Total DRP1 was analyzed by Western blot (e, f). U87MG cells were transfected with siBeclin–1 and the expression of TOM20 and COXIV was analyzed by confocal microscopy (g, h) and Western blot (i) respectively. U87MG cells were treated with AGG in the presence of 3-MA (5 mM, 2 h) and CQ (20 μM, 2 h) and TOM20 expression was quantified by confocal microscopy (j-m). The data were reported as the mean ± S.D. of three independent sets of the experiment and compared to PBS control. *P-value < 0.05; **P-value < 0.01 were considered significant. #P-value < 0.05 was considered significant as compared to the AGG treated group. Densitometry was performed on the original blots, considering that the ratio of protein to actin in control cells was 1.

increase in red mKeima-Red-Mito7 puncta per cell was found in AGG-treated U87MG cells as compared with control (Fig. 3a, b) which is confirmatory of the fact that AGG-prompted mitochondrial damage leads to mitophagy for mitochondrial clearance.

3.2. AGG activates class III PI3K around depolarized mitochondria

Next, we investigated if AGG-induced dysfunctional mitochondria are required for induction of mitophagy. After AGG treatment in U87MG cells, healthy and dysfunctional mitochondria were analyzed by flow cytometry using MitoTracker Green FM and MitoTracker Red CMXROS labels, respectively. The results showed that an exposure to AGG leads to an upregulation of the percentage of damaged mitochondria in U87MG cells (Fig. 4a). Further, we analyzed the activation of class III PI3K around depolarized mitochondria in AGG treated U87MG cells. To evaluate this factor, we transfected the cells with a plasmid that expressed a p40(phox)PX–EGFP fusion protein. As the PX domain of p40(phox) is known to specifically interact with the product of class III PI3K-phosphatidylinositol 3-phosphate (PtdIns-3-P), p40(phox)PX–EGFP serves as a probe for evaluating the subcellular level and distribution of PtdIns–3-P [32]. After exposure to AGG the transfected cells were stained with TOM20 and analyzed by confocal microscopy. The data generated by this experiment supported our hypothesis as it was observed that mitochondrial staining was diminished in AGG treated U87MG cells and that the remaining mitochondria were concentrated in perinuclear clusters that were apposed with p40(phox) PX–EGFP hotspots (Fig. 4b and c).

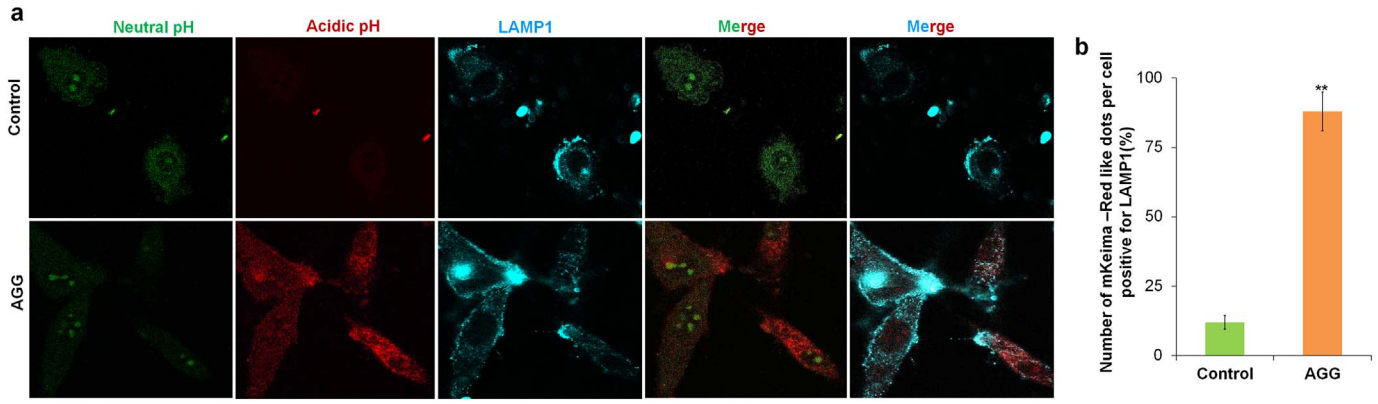

Fig. 3. Effect of AGG on fusion of mitophagosome and lysosome in U87MG cells. U87MG cells were transfected with mKeima-Red-Mito7 for 48 h and stained with LAMP1 after 24 h AGG treatment and colocalization was studied by confocal microscopy (a, b). The data reported as the mean ± S.D. of three independent experiments and compared to the PBS control. **P-value < 0.01 was considered significant.

3.3. AGG induces mitophagy through disruption of mitochondrial bioenergetics

One of the major causes of mitochondrial dysfunction is the alteration in the mitochondrial bioenergetics pattern. To test our hypothesis that AGG exerts its effect in a similar fashion, we measured the oxygen consumption rate (OCR) and ATP depletion in U87MG cells. A dose and time dependent reduction was seen in the oxygen consumption activity in AGG treated cells as compared to control U87MG cells (Fig. 4d and e). Additionally, the results showed that ATP generation was reduced in the presence of AGG as compared to control U87MG cells (Fig. 4f). This indicates that inhibition of OCR together with the reduction in ATP concentration may result in the generation of dysfunctional mitochondria which in turn primes the cell for mitophagy. Besides that, our study failed to uncover any significant difference in the rate of glycolytic flux between control and AGG treated cells; more importantly, it was noted that the fall in ATP cannot be compensated through glycolysis (Supplementary Fig. S5a and b) suggesting that AGG induced dysfunctional mitochondria are responsible for the disturbance in the energy homeostasis and therefore, induction of mitophagy. In further support for the hypothesis, our study also failed to find any correlation between dose dependency and extracellular acidification rate (ECAR) (Supplementary Fig. S5c and d). To test whether the dysfunctional mitochondria generation could be reversed by increasing OCR, we exogenously provided an energy supplement—methyl pyruvate (MP), a cell-permeable form of pyruvate. Interestingly, MP supplementation was observed to rescue dysfunctional mitochondria by increasing their OCR (Fig. 4g); more importantly, MP supplementation was seen to effect a decrease in the ROS levels (Fig. 4h) suggesting that ROS plays a crucial role in regulating mitochondrial bioenergetics status during AGG induced mitophagy. To verify our hypothesis, we investigated mitochondrial culling by TOM20 analysis in MP supplemented AGG treated cells. The abrogation of mitophagy was observed in MP supplemented AGG treated cells when compared to exclusively AGG insulted cells (Fig. 4i and j).

3.4. PUMA, the central regulator of AGG, induces mitochondrial garbage disposal

The activation of PUMA, BH3 only proapoptotic protein, is associated with DNA damage-mediated apoptosis (Supplementary Fig. S2 and S3) [14]. In this study, we used immunofluorescence and Western blot analysis to show that an exposure to AGG increased the expression of PUMA in a dose-dependent manner (Fig. 5a–c). To investigate whether PUMA could play a role in the degradation of depolarized mitochondria, we immunostained AGG-exposed cells for both PUMA and TOM20 and studied the colocalization between the two using confocal microscopy. The results revealed the formation of an intense yellow color in perinuclear region confirming that PUMA co-localizes with TOM20. We also observed that the proportion of cells that were positive for both PUMA and TOM20 was significantly higher in AGG treated cells as compared to the control (Fig. 5d and e). This indicates that PUMA is recruited to the cluster of damaged mitochondria around the nucleus possibly for forming mitophagosomes for degradation. Further, we analyzed the involvement of PUMA in mitophagy through gain and loss of function studies (Supplementary Fig. S4b and c) in the presence of AGG. The data showed that there was a significant increase in mitochondrial TOM20 staining in siPUMA as compared to sicontrol U87MG cells which proves that knocking down PUMA inhibited AGG-induced mitophagy (Fig. 5f and g). In addition, the transient overexpression of PUMA in AGG treated cells resulted in a decrease in the mitochondrial TOM20 staining expression as compared to mock control groups (Fig. 5h and i). In the light of the above findings, we quantified the percentage of healthy and dysfunctional mitochondrial mass in both PUMA overexpressed as well as knock down conditions in AGG treated U87MG cells. It was observed that in comparison to the control groups, the percentage of depolarized mitochondria mass was higher and that of the healthy mitochondrial mass was lower in PUMA overexpressed and deficient cells, respectively, when they were exposed to AGG (Fig. 6a and b). To strengthen these findings, we quantified the OCR and ATP generation. The data revealed that AGG-induced abrogation in OCR and ATP was altered in the case of knock down or overexpressed condition (Fig. 6c–f). This confirms that PUMA triggers mitophagy by disturbing mitochondrial energy demands.

3.5. PUMA contains LC3 interacting region motif crucial for AGG-induced mitophagy

It is well established that mitophagy receptors interact with the autophagosomal associated protein LC3 in order to direct dysfunctional mitochondria toward autophagic degradation. For instance, BH3-only proteins such as BNIP3 and Nix accomplish autophagic degradation of mitochondria by interacting with LC3 through their LC3-interacting region (LIR) motifs [6,10]. In our setup, the sequence analysis showed that Tyr172, Asn173, Leu174, and Ile175 residues of PUMA could be functioning as the LIR motif (Fig. 7a and b). To understand the interactions between the LC3 domain and hPUMA, 15 ns long Molecular Dynamics (MD) simulation of the docked LC3-hPUMA complex was performed. The results indicated that the complex was sufficiently stable (Fig. 7c) with Cα atoms root mean square deviations (RMSD) value of 3 to 4.5 Å according to the MM-GBSA based average binding free energy (Supplementary Fig. S6). The detailed contributions from various energy components were calculated for the complex by taking 500 snapshots from the last 5 ns of the MD trajectory as was shown in

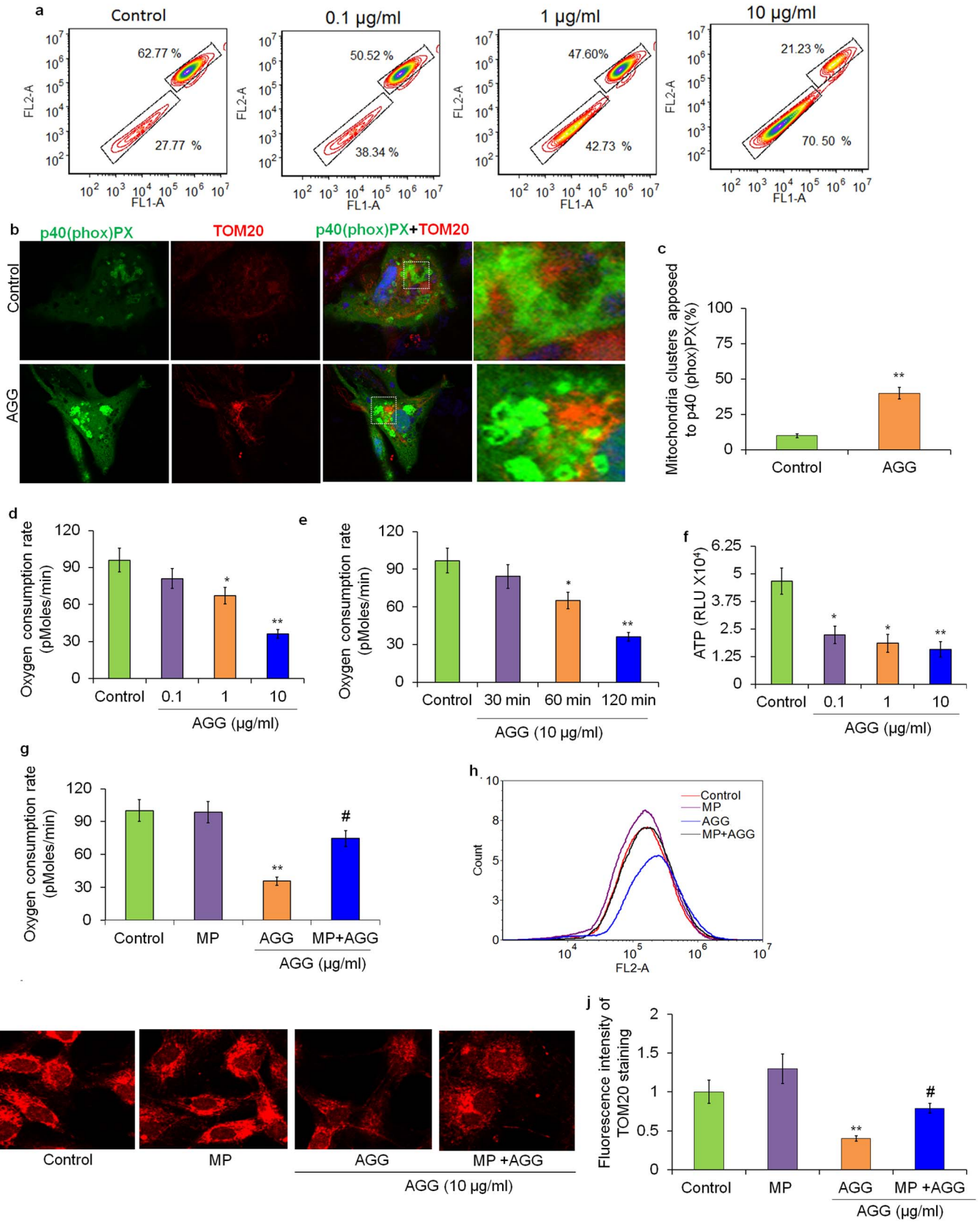

Fig. 4. AGG activates class III PI3K around depolarized mitochondria to induce mitophagy. U87MG cells were treated with AGG and mitochondrial dysfunction was performed through flow cytometry (a). U87MG cells were transfected with p40(phox)PX–EGFP and stained with TOM20 after AGG treatment and analyzed in confocal microscopy (b). The graph represents mitochondrial clusters apposed to p40(phox)PX (c). U87MG cells were treated with AGG for 24 h and, oxygen consumption rate (d, e) and ATP (f) were quantified. U87MG cells were treated with AGG in the presence of methyl pyruvate (MP, 1 mM, 2 h) and OCR (g), ROS through flow cytometry (h) and expression of TOM20 (i, j) were quantified. The data reported as the mean ± S.D. of three independent experiments and compared to the PBS control. *P-value < 0.05, **P-value < 0.01 were considered significant. #P-value < 0.05, was considered significant as compared AGG treated group.

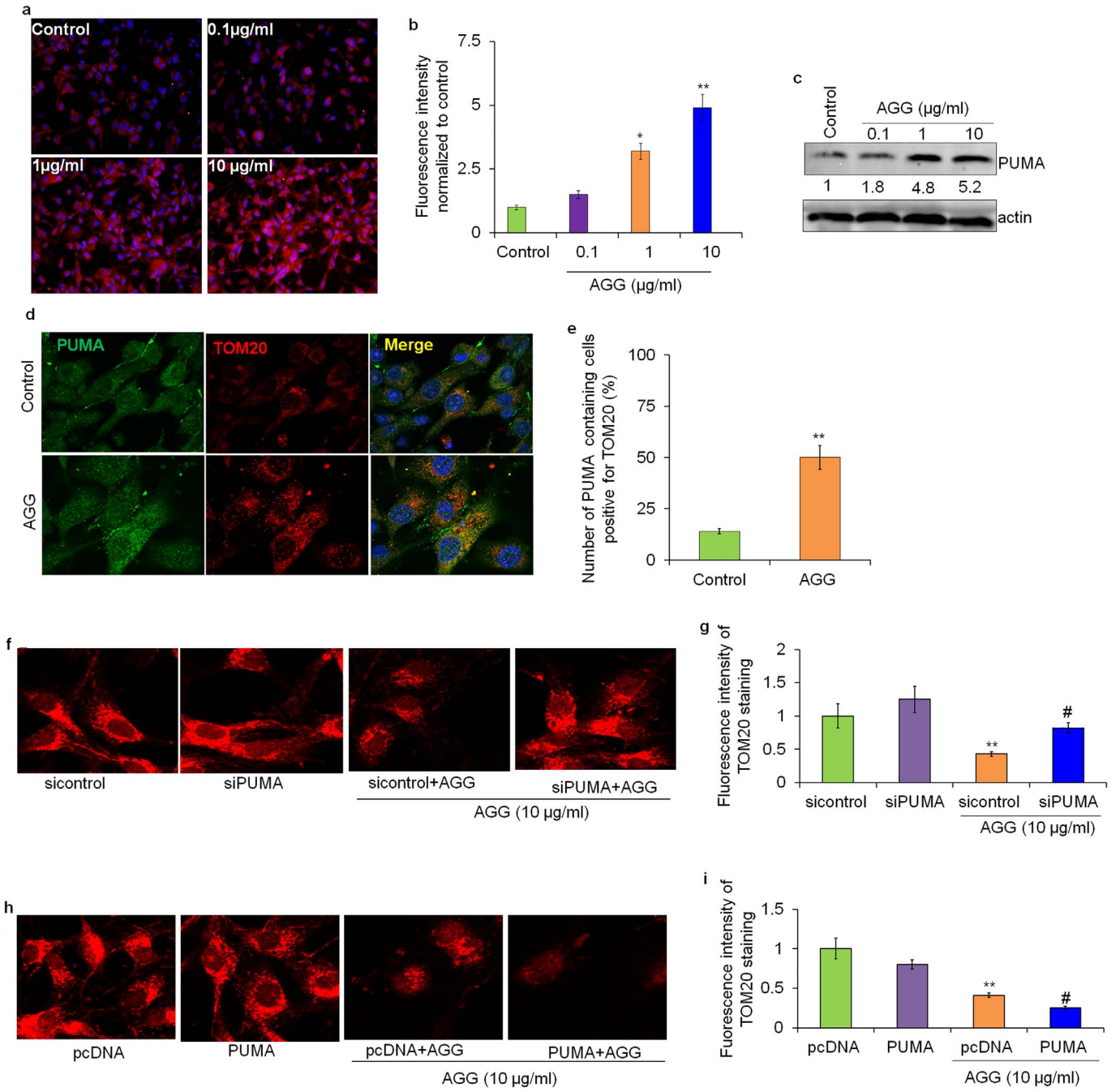

Fig. 5. PUMA regulates AGG-induced mitophagy. U87MG cells were treated with AGG for 24 h and the expression of PUMA was measured by fluorescence microscope (a, b) and Western blot (c). U87MG cells were stained with PUMA and TOM20 after AGG treatment and recruitment of PUMA in damaged mitochondria was analyzed by confocal microscopy and the graph indicates that PUMA containing cells were positive for TOM20 (d, e). U87MG cells were knocked down with siPUMA and overexpressed with PUMA containing plasmids and the expressions of TOM20 in AGG treated cells were quantified by confocal microscopy (f-i). The data reported as the mean ± S.D. of three independent experiments and compared to PBS control. *P-value < 0.05, **P-value < 0.01 were considered significant. #P-value < 0.05 was considered significant as compared AGG treated group.

supplementary section Table S1. The calculated binding free energy of the complex was determined to be − 45.218 kcal mol^{-1} as per the MM-GBSA method. The favorable contributions from the direct electrostatic interactions between hPUMA domain and LC3 were recompensed for by the electrostatic de-solvation free energy upon binding. As a whole, the contribution was determined to be unfavorable, being consistent with other MM-GBSA and MM-PBSA studies. By contrast, in nonpolar interactions, $\Delta G_{nonpolar}$ (including van der Waals interactions and nonpolar solvation) contribute − 131.898 kcal mol^{-1}, which is very favorable toward the binding process and consistent with the large hydrophobic binding surface that is present between the hPUMA domain and LC3. By decomposing the binding free energy into the contribution from each residue, it was likely to recognize the binding hotspots for hPUMA domain and LC3 (Fig. 7d). The results indicated that several residues of the LC3 domain (Arg10, Glu14, Glu18, Asp19, Leu22, Ile23, Phe52, Leu53, and Ile66) favorably contribute greater than − 1.5 kcal mol^{-1} of the free energy. Additionally, certain other residues, such as Glu25, Gln26, and Pro55, contribute also contribute about − 1 kcal mol^{-1} of the free energy. Upon comparison, it can be seen that these key residues of the LC3 domain that are crucial for interacting with hPUMA are located on one of the four anti-parallel beta sheets present and the longer α-helix, which together form a ridge-like

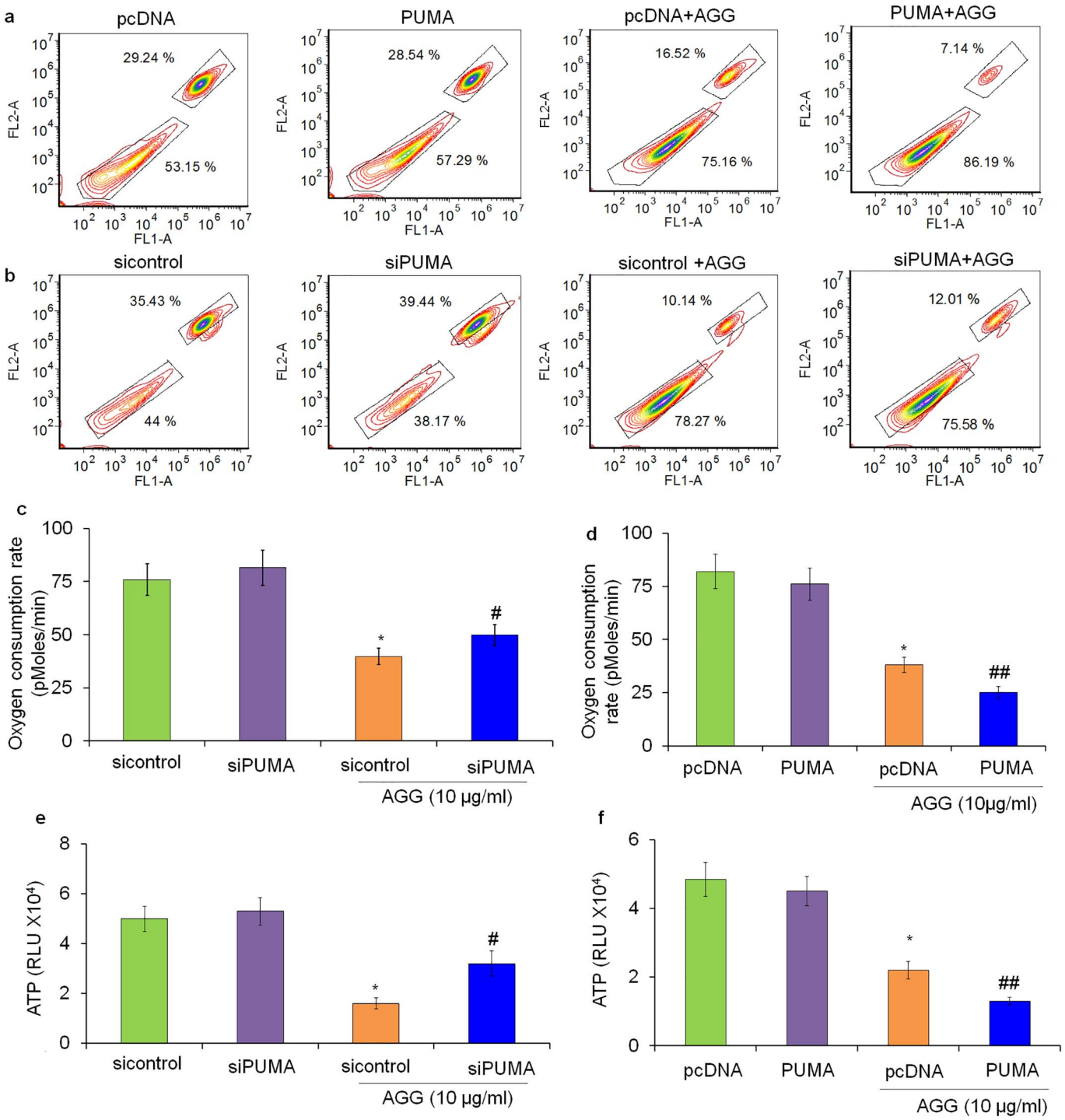

Fig. 6. PUMA regulates AGG-induced mitochondrial bioenergetics to activate mitophagy. U87MG cells were knocked down with siPUMA and overexpressed with PUMA plasmid and treated with AGG for 24 h. The dysfunctional mitochondria through flow cytometry (a, b), OCR (c, d) and ATP (e, f) were analyzed in U87MG cells. The data were reported as the mean ± S.D. of three independent sets of the experiment and compared to PBS control. *P-value < 0.05 was considered significant. #P-value < 0.05, ##P-value < 0.01 were considered significant as compared AGG treated group.

structure (Fig. 7e). The residue energy decomposition results for hPUMA showed that Ser36, Gln157, Gln161, Arg162, Arg169, Tyr172, Asn173, Met176, Leu181, Pro182, and His185 each contribute more than $-1.5\ \text{kcal mol}^{-1}$ of the free energy, while Lys40, Glu41 and Pro42 contribute about $-1\ \text{kcal mol}^{-1}$ of the free energy. These important residues were located toward the end of the large α-helix and the second helix in the C-terminal region of hPUMA (Fig. 7f).

The above-mentioned findings were validated through co-immunoprecipitation as well as confocal microscopic colocalization studies. Co-immunoprecipitation results revealed that AGG-triggered PUMA strongly interacted with LC3 in order to induce mitophagy in U87MG (Fig. 7g). To gain additional insight, the U87MG cells were co-transfected with hLC3WT as well as EGFP-PUMA and the co-localization studies were conducted through confocal microscopy. A strong yellow color in AGG treated U87MG cells were seen, indicating that PUMA interacts with the LC3 protein. Importantly, the number of LC3 dots per cell positive for PUMA increased significantly in the AGG treated group as compared to control cells (Fig. 7h and i). To verify

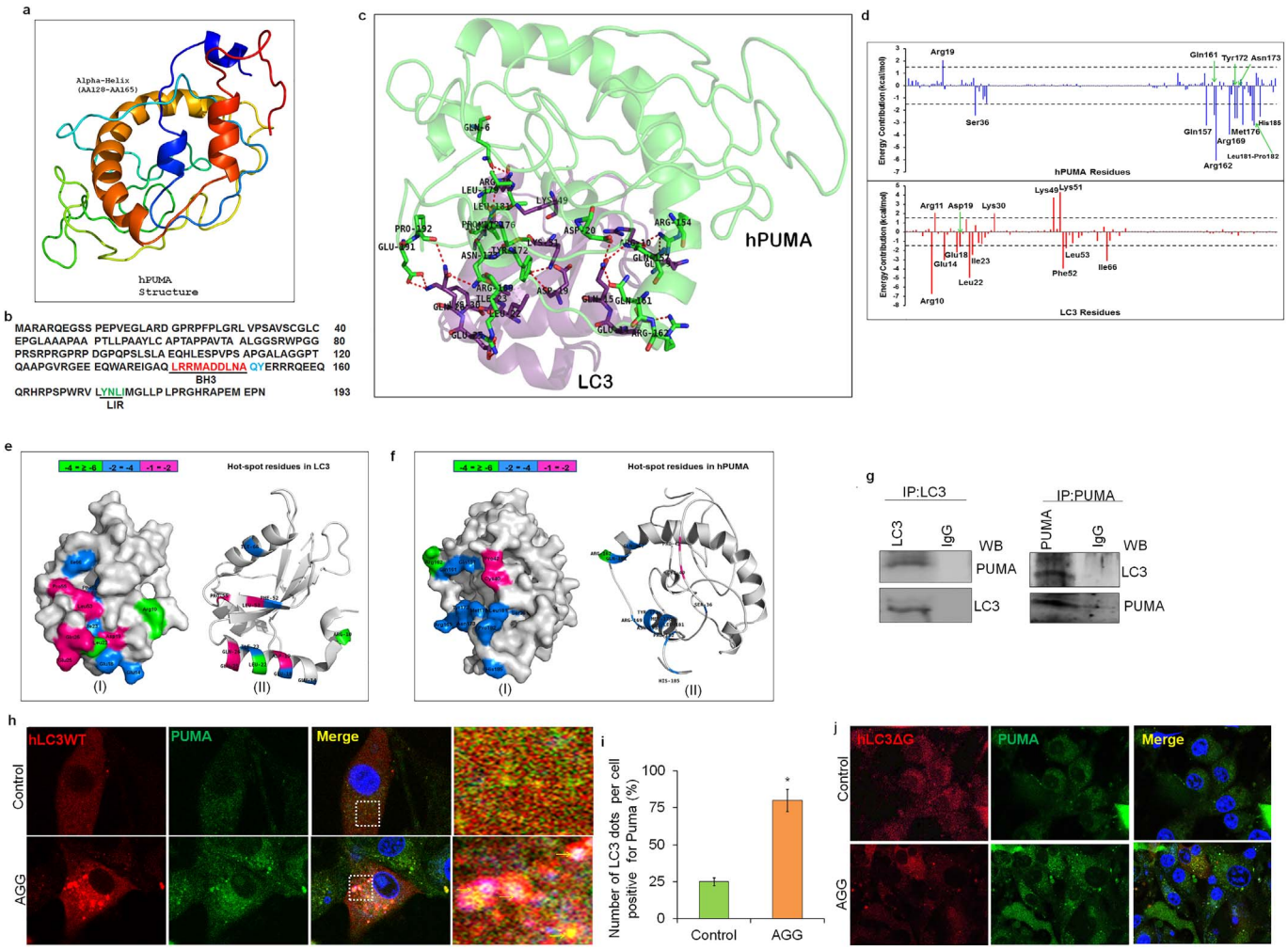

Fig. 7. PUMA contains LIR to interact with LC3. The schematic ribbon representation of the predicted structure of hPUMA from *ab initio* modeling by PHYRE–2 software (a) and the sequence of BH3 (red), LIR (green) and ubiquitination residues (cyan) (b). A schematic ribbon representation of the LC3-hPUMA complex structure is shown in different colors. LC3 domain is shown in violet color while the hPUMA structure is shown in green color. The residues indicating the interactions are shown at sticks along the domain interface for both LC3 and hPUMA (c). The decomposition of ΔG on per residue basis or the pair interaction energy between LC3 domain and hPUMA: the contribution of each residue in hPUMA to LC3 domain binding and the contribution of each residue in the LC3 domain to hPUMA binding (d). The distributions of the identified hotspot residues on the LC3 (e) and PUMA (f) domain as a (I) surface representation and (II) cartoon representation. Colored bars show the range of contributions by the residues in the unit kcal/mol. U87MG cells were treated with AGG for 24 h and immunoprecipitated with anti–LC3 and anti-PUMA followed by immunoblotting with anti–PUMA or anti–LC3 antibodies (g). U87MG cells were co-transfected with vectors encoding mCHERRY-hLC3 and EGFP-PUMA followed to treat with AGG for 24 h and colocalization was studied through confocal microscopy (h, i). U87MG cells were co-transfected with the vectors encoding mCHERRY-hLC3ΔG and EGFP-PUMA and treated with AGG for 24 h. The colocalization was studied through confocal microscopy (j). The data were represented as mean ± SD and *P-value < 0.05 was considered significant.

whether lipidated LC3 is necessary for induction of mitophagy in AGG treated U87MG cells, the cells were transfected with the hLC3ΔG construct, in which, the C-terminal Gly(120) residue that is deemed essential for LC3-lipidation was deleted. It was observed that the co-transfection of hLC3ΔG and EGFPPUMA did not show any significant co-localization between PUMA and mutant LC3 in AGG treated U87MG cells (Fig. 7j), which suggests that PUMA specifically binds with LC3-II for degradation of damaged mitochondria.

3.6. PUMA ubiquitination facilitates AGG-prompted mitochondrial slaughtering

Selective mono and poly-ubiquitination of mitochondrial membrane proteins recruit p62, which in turn interacts with LC3 in order to induce mitophagy for clearance of damaged mitochondria [2,4]. It is hypothesized that for this process ubiquitination of PUMA might be an important step that is required for priming the mitochondria undergoing mitophagy in AGG treated cells. Previous studies have shown that for proteosomal degradation the PUMA protein is required to be ubiquitinated at the Gln151 and Tyr152 residues located in N-terminal region [33]. Our study explored this hypothesis and analyzed if AGG induced PUMA localized in mitochondria required ubiquitination for the induction of mitophagy. The data showed that exposure to AGG promoted a strong co-localization between ubiquitin and PUMA as evidence by the appearance of an intense yellow color in the cells; in contrast, a very diffuse co-localization was observed in control U87MG cells that were not exposed to AGG (Fig. 8a and b). The ubiquitinated status of PUMA was further confirmed by immunoprecipitation studies, which revealed that the expression of ubiquitinated PUMA in the AGG treated group was significantly higher than that found in control U87MG cells. (Fig. 8c). Intriguingly, when immunoprecipitation studies were conducted on the cells that had been pretreated with PYR41 (inhibitor of the ubiquitin-activating enzyme), a reduction in the interaction of ubiquitin with PUMA in AGG exposed U87MG cells was observed (Fig. 8d). In order to decipher if this phenomenon was relevant for AGG induced mitophagy in U87MG cells, we further investigated this observation. Surprisingly, it was observed that pretreatment with Pyr41 in AGG treated cells did not significantly change in

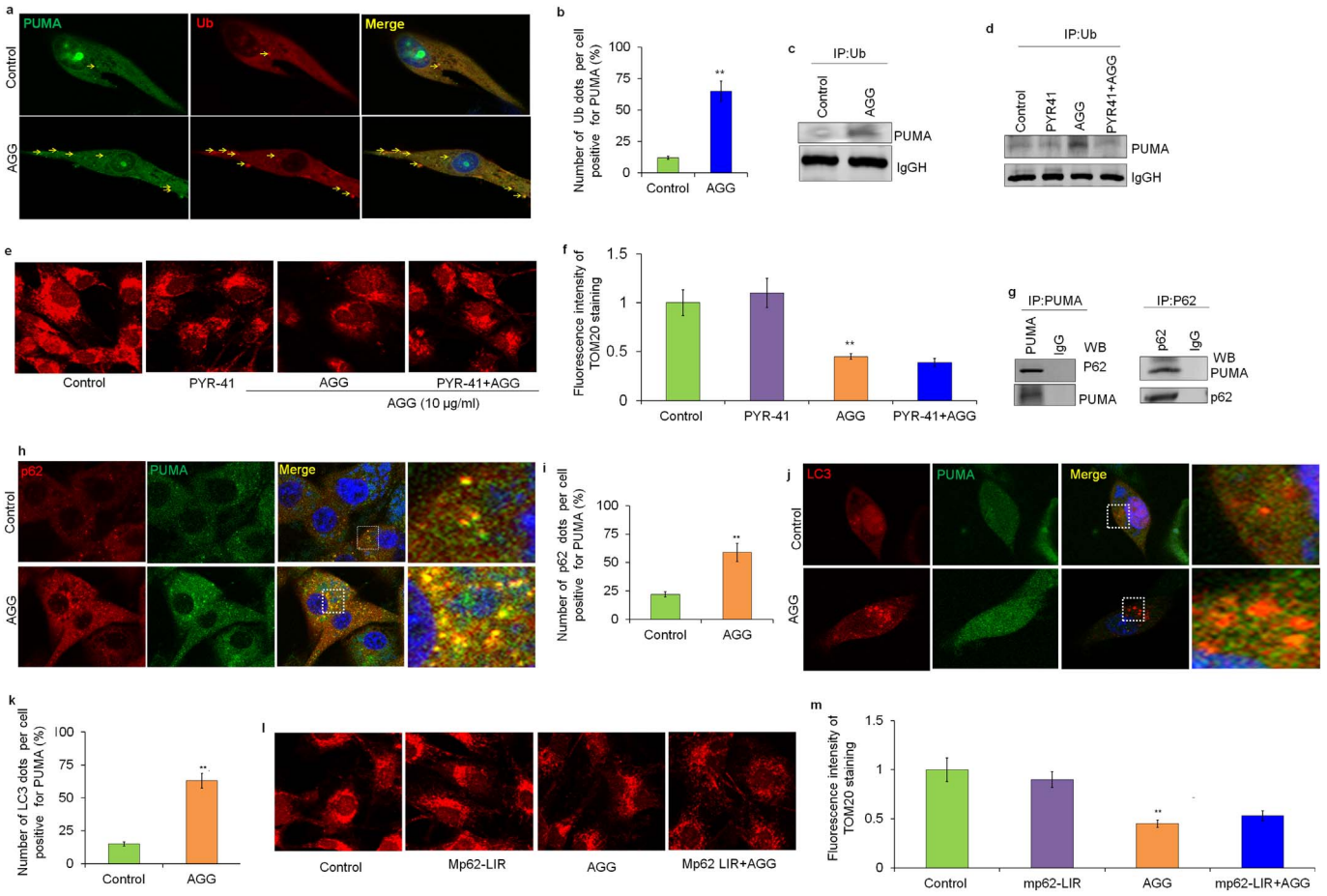

Fig. 8. PUMA ubiquitination facilitates AGG-prompted mitochondrial slaughtering. After AGG treatment U87MG cells were stained with ubiquitin and PUMA and the colocalization was studied through confocal microscopy (a, b). U87MG cells were treated with AGG in presence of PYR–41 (1 μM, 2 h) and PUMA/Ub interaction was studied by immunoprecipitation analysis (c, d) and the expression of TOM20 was analyzed through confocal microscopy (e, f). U87MG cells were treated with AGG for 24 h and immunoprecipitated with anti–p62 and anti-PUMA followed by immunoblotting with anti–PUMA or anti–p62 antibodies (g). After AGG treatment, U87MG cells were stained p62 and LC3 and colocalization was studied through confocal microscopy (h, i). U87MG cells were transfected with p62 LIR mutant and stained with PUMA and LC3 after AGG treatment and analyzed for colocalization between PUMA and LC3 through confocal microscopy (j, k) and expression of TOM20 was analyzed through confocal microscopy (l, m). The data were reported as mean ± S.D. of three independent sets of the experiment and compared with the PBS control. **P-value < 0.01 was considered significant.

mitochondrial staining when compared to AGG treated cells (Fig. 8e and f). This is indicative of the existence of more than one mechanism for the induction of mitophagy in the case of an AGG insult. In this specific case, we postulate that the inhibition of ubiquitination-dependent mitophagic pathway was compensated for by the direct association of PUMA with LC3 which served as an alternative pathway for mitophagy.

After noticing a strong colocalization between PUMA and ubiquitin, we investigated the interaction between PUMA and p62 which is a selective adapter molecule for autophagy. The co-immunoprecipitation study was performed to pull out p62 and PUMA from AGG-treated U87MG cell lysates using anti-PUMA or anti-p62 antibodies for immunoprecipitation followed by immunoblotting with anti-p62 or anti-PUMA antibody (Fig. 8g). The results revealed that PUMA interacts with p62 in AGG treated cells, which confirms that p62 acts as a bridge for connecting ubiquitinated mitochondria with LC3. Additionally, the confocal analysis showed the colocalization of p62 with PUMA in AGG treated cells in comparison to control in U87MG cells (Fig. 8h and i). Further, our study probed the contribution of p62 in AGG induced mitophagy. A p62 LIR mutant (W338A) was transfected in U87MG cells and colocalization of PUMA and LC3 was examined by confocal microscopy. The results revealed that AGG induced PUMA and LC3 colocalization did not get affected and the percentage of LC3 dots per cell, *i.e.*, positive for PUMA, was notably enhanced as compared to the control in p62 LIR mutant U87MG cells (Fig. 8j and k). Furthermore, it was clearly observed that fluorescence intensity in mitochondrial staining remained unaltered in AGG exposed p62 LIR mutant U87MG cells as compared to AGG alone (Fig. 8l and m). This was in accordance with previous reports, wherein it was established that p62 is dispensable in the Parkin-induced mitophagy in which it functions primarily for mitochondrial clustering but not for mitophagy [34]. It is tempting to hypothesize that p62 is not necessarily important for AGG induced mitophagy and suggest that AGG induced mitophagy follows multiple pathways for clearance of mitochondrial trafficking. Phosphatase and tensin homolog deleted on chromosome 10-induced kinase 1 (PINK1) is a serine/threonine kinase which remains stabilize on outer membrane of depolarized mitochondria to recruit Parkin during the mitophagy induction. To illustrate whether Parkin has any role in AGG-induced mitophagy, we have analyzed TOM20 degradation as change in expression of TOM20 in HeLa cells lacking Parkin after AGG (10 μg/ml) insult (Fig. 9a, b). Interestingly, we failed to notice any significant difference in TOM20 staining after 24 h treatment of AGG in HeLa cells along with CCCP. In Parkin-expressing HeLa cells, AGG was shown to trigger mitophagy as accessed by TOM20 staining confirming AGG induces Parkin-dependent mitophagy (Fig. 9c, d). In this connection, we knock down Parkin in U87MG cells (Fig. 9e) and analyzed any alteration in mitophagy in presence of AGG. Our data showed that AGG could not decline the expression of TOM20 staining in Parkin deficient U87MG cells as compared to only AGG treated cells (Fig. 9f, g) concluding mitophagy induced by AGG mediates through Parkin in U87MG cells.

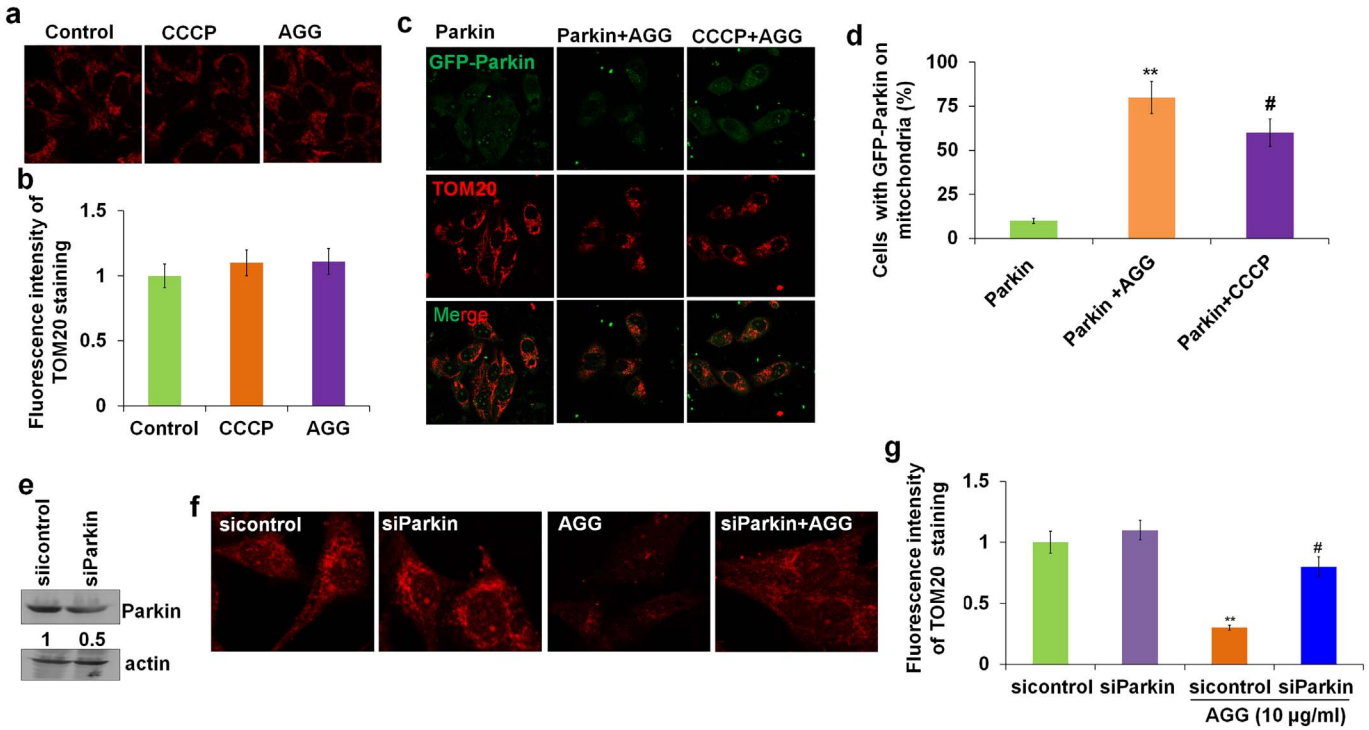

Fig. 9. AGG induces Parkin dependent mitophagy in U87MG cells. HeLa cells were treated with AGG (10 µg/ml) for 24 h and CCCP (10 µM) for 1 h and stained with TOM20 and analyzed through confocal microscopy (a, b). HeLa cells were over-expressed with plasmid containing Parkin followed to 24 h AGG treatment and intensity of TOM20 was analyzed through confocal microscopy (c, d). U87MG cells were transfected with siParkin for 48 h (e) and TOM20 expression was analyzed after 24 h AGG treatment (f, g). The data were reported as the mean ± S.D. of three independent sets of the experiment and compared to PBS control. *P-value < 0.05, **P-value < 0.01 were considered significant. #P-value < 0.05, ##P-value < 0.01 were considered significant as compared AGG treated groups.

3.7. Ceramide acts as an upstream signal in AGG-induced mitophagy and apoptosis

Ceramide is a bioactive sphingolipid that is known to play a key role in controlling various cellular mechanisms such as autophagy and apoptosis [30,35]. The accumulation of ceramide, especially in mitochondria in which it plays a critical role in ceramide-induced stress, accelerates the formation of fragmented and dysfunctional mitochondria. AGG has been shown to activate ER stress and ROS generation as a mean to modulate various tumor suppressor activities. In this study, we aimed to identify if examined AGG could generate ceramide and if there exists a relationship between AGG, ceramide, ER stress and ROS generation vis-à-vis mitophagy. Initially, ceramide generation by AGG in U87MG cells was quantified using anti-ceramide through fluorescence microscopy. The data showed that AGG triggered the ceramide production in a dose and time-dependent manner (Fig. 10a–d). Furthermore, we uncovered that AGG-induced synthesis of ceramide was decreased in the presence of myriocin–1 (ISP–1), which is an inhibitor of serine palmitoyltransferase (SPT) (Fig. 10e and f). Next, we analyzed the detailed molecular pattern underlying ceramide synthesis by AGG through mass spectroscopic analysis of U87MG cells. The data showed that in comparison to control, the levels of different long-chain ceramide species, including those with C14, C16, C18, C20, C22, and dihydro-C16-ceramide (dhC16-Cer) backbone, were significantly upregulated in a dose-dependent manner when U87MG cells were exposed to AGG (Fig. 10g). It is well established that mammalian ceramide synthases 1–6 (CerS1 to CerS6) are involved in the synthesis of ceramides of different chain lengths. CerS1 expression is associated with the C18-ceramide generation which is implicated in the mitophagy process. A previous study reported that there occurs a direct interaction between C18-ceramide and LC3B-II on mitochondrial membrane for induction of mitophagy [30]. In line with this observation, our study showed that exposure to AGG increased the expression of endogenous C18-ceramide, which in turn induced mitophagy in U87MG cells (Fig. 10g). Further, U87MG cells were treated with RITC labeled AGG, stained with CerS1 and analyzed through confocal microscopy. The results showed that AGG exhibited strong co-localization with CerS1 as evidenced by the formation of an intense yellow color in the cells (Fig. 10h). Interestingly, we found that the exposure to AGG increased the expression of CerS1 substantially in dose-dependent manner (Fig. 10i and j) which indicates that AGG-activated CerS1 is associated with the generation of C18-ceramide during the process of mitophagy induction.

ER stress and ROS have been shown to be associated with regulation of AGG induced autophagy [26] and apoptosis [23,24], respectively. In this study, we probed the possibility that AGG induced mitophagy was modulated by ROS and/or ER stress, and examined its relationship with the synthesis of ceramide. As an initial step, we examined the induction of mitophagy in the presence of ISP–1, which is a known ceramide inhibitor. The data revealed that as compared to the control group which was treated with only AGG, the test group demonstrated that, in the presence of ISP–1, the AGG-induced decrease in TOM20 expression was upregulated (Fig. 11a and b). Furthermore, it was seen that upon pretreatment with salubrinal and NAC, the AGG-mediated decrease in TOM20 expression was restored (Fig. 11c–f). Additionally, AGG-triggered apoptosis and autophagy were both suppressed in the presence of ISP–1 as demonstrated by a decrease in caspase 3/7 activity (Fig. 11g) and a decrease in the accumulation of cleaved PARP and LC3 (Fig. 11h), respectively. It is likely that both AGG-activated ER stress as well as GRP–78 expression were suppressed in the presence of ISP–1 (Fig. 11h). In addition, the pretreatment with ISP–1 prevented AGG-induced ROS generation (Fig. 11i) and decreased the OCR (Fig. 11j) establishing that the ceramide generation process is upstream of AGG associated ER stress and ROS accumulation promotes mitochondrial damage and mitophagy.

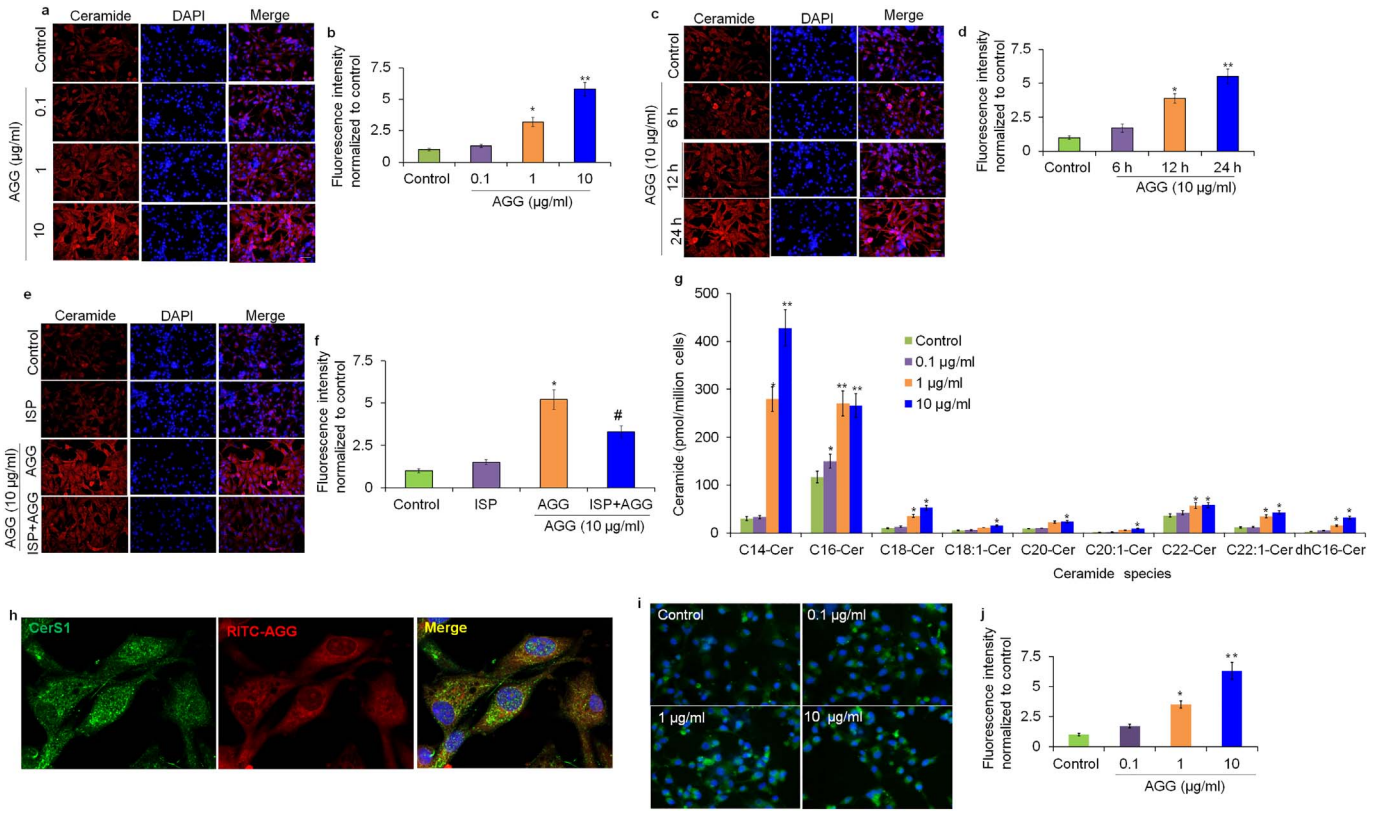

Fig. 10. Ceramide acts as an upstream signal in AGG-induced mitophagy and apoptosis. U87MG cells were treated with AGG as indicated and the expression of ceramide was quantified using anti-ceramide antibody through fluorescence microscopy (a-d). U87MG cells were treated with AGG in the presence of ISP–1(10 μM, 2 h) and the expression of ceramide was quantified using anti-ceramide antibody through fluorescence microscopy (e-f). U87MG cells were treated with different concentrations of AGG for 24 h and ceramide species were determined using Mass Spectrometry (g). The results are presented as ceramide levels (pmol/million cells). U87MG cells were treated with RITC-AGG for 6 h and stained with CerS1 and colocalization was studied by confocal microscopy (h). U87MG cells were treated with AGG for 24 h and the expression of CerS1 was examined through fluorescence microscopy (I, j). The data were reported as the mean ± S.D. from three independent sets of experiment and compared to PBS control. *P-value < 0.05; **P-value < 0.01 were considered significant. #P-value < 0.05 was considered significant as compared AGG treated groups.

3.8. AGG induces mitophagy that culminates in apoptosis

Mitophagy may be either cytoprotective or lethal depending on cellular context. In this study, we investigated whether AGG induced mitophagy is associated with cell death. In this regard, the mitophagy-inducing activity of AGG was analyzed in the presence of the mitochondrial division inhibitor–1 (Mdivi–1), which inhibits DRP1-GTPase activity thereby disrupting the mitochondrial fission process. Our data showed that AGG-induced mitophagy was strongly inhibited in the presence of Mdivi–1 (Fig. 12a and b), which confirms that AGG-mediated mitophagy is a DRP1 dependent process. Furthermore, U87MG cells were treated with AGG in the presence of Mdivi–1, and both cell viability and apoptosis induction were studied. The data showed that the AGG-mediated decrease in the cell viability was enhanced in the presence of Mdivi–1 (Fig. 12c), which indicates that the inhibition of mitophagy also suppressed cell death. Interestingly, the pretreatment with Mdivi–1 reduced caspase (3/7) activity as compared to control cells (Fig. 12d). The findings outlined above suggest that although AGG induced mitophagy is essential in terms of maintaining cellular homeostasis, excessive mitophagy due to AGG insult results in the disruption of mitochondrial bioenergetics as well as mitochondrial membrane collapse leading to apoptotic cell death.

4. Discussion

Mitochondrial autophagy or mitophagy is a selective form of autophagy in which mitochondria are selectively targeted for degradation in autolysosomes. Basal levels of mitophagy are important for maintaining cellular homeostasis and protecting cells against accumulation of dysfunctional mitochondria, thus maintaining the integrity of the mitochondrial pool [3,4]. Many mitophagic receptors from the BH3 family proteins have been identified for the maintenance of normal cellular functions [6,10]. For example, Nix induces mitophagy in order to eliminate mitochondria during the late phase of erythrocyte maturation [6]. However, under conditions that involve overwhelming mitochondrial damage, apoptosis becomes dominant and the inactivation of critical proteins of the autophagy pathway allows for the induction of cell death [7,15,36,37]. Likely, ceramide functions as a receptor for LC3-II in order to induce lethal mitophagy at the mitochondrial membrane [30]. In this study, we show for the first time that in glioma cells AGG-induced ceramide eliminates excessive, superfluous or damaged mitochondria through mitophagy and disrupts cellular homeostasis which then switches to apoptosis. Additionally, we have identified AGG-induced PUMA as the mitophagy receptor essential for clearing dysfunctional mitochondria.

Mitochondrial autophagy is triggered against oxidative stress, hypoxia, metabolic alteration, and the accumulation of protein aggregates [4,8]. In this study, oxidative stress-dependent mitochondrial dysfunction has been shown to be a key factor for AGG induced mitophagy. Interestingly, supplementing with methyl pyruvate was seen to rescue cells from oxidative stress and mitophagy, thereby confirming the hypothesis. It has recently been reported that in HepG2 cells, amitriptyline, which is a tricyclic antidepressant, was capable of inducing mitophagy through oxidative stress mediated mitochondria dysfunction and that the treatment with antioxidants was seen to suppress mitophagy [38]. In this regard, our study has shown that AGG-induced PUMA regulates mitochondrial metabolic activity for the induction of mitophagy. The protein sequence of PUMA contains a conserved

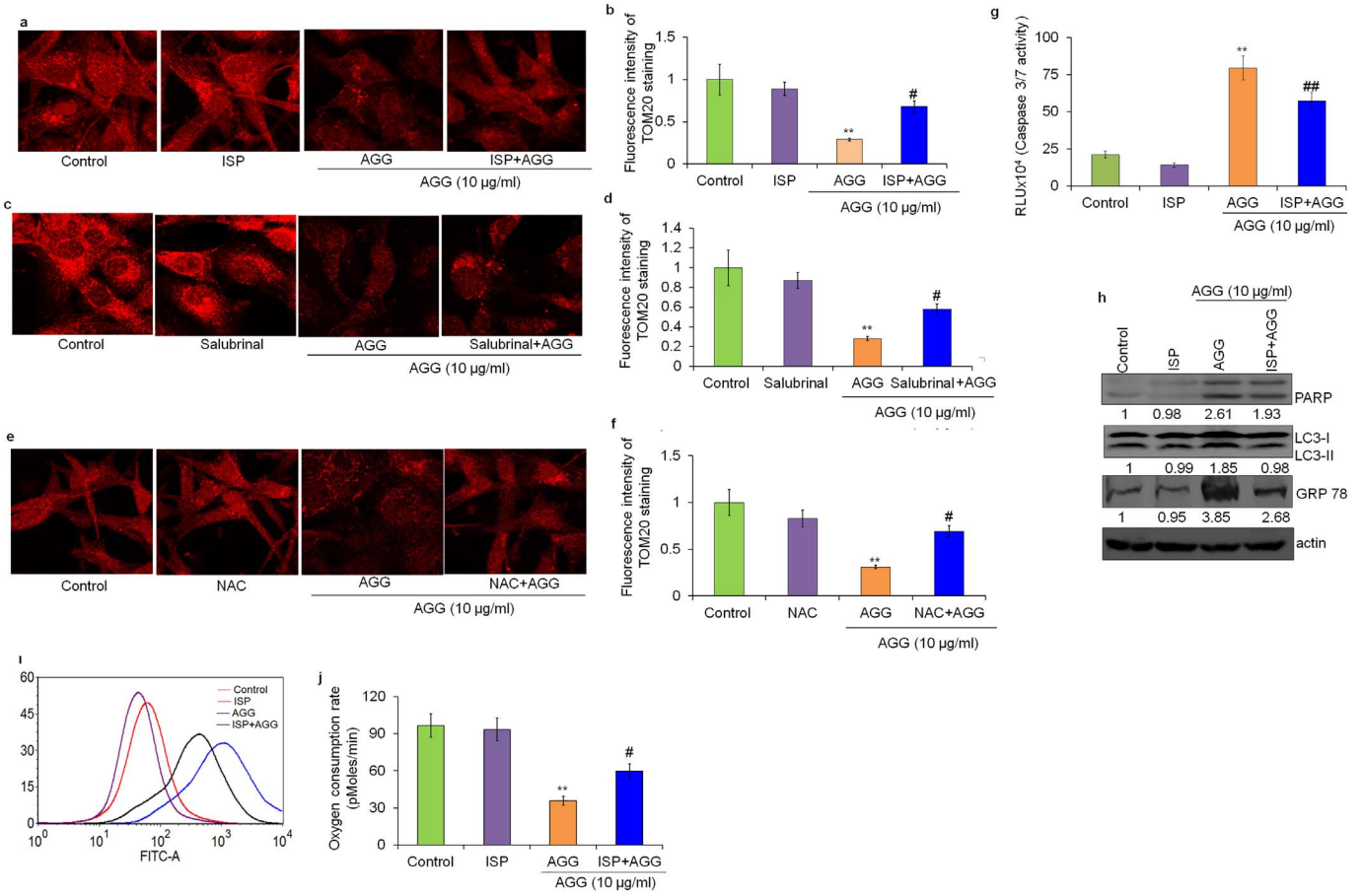

Fig. 11. AGG induced ceramide regulates autophagy and apoptosis. U87MG cells were treated with AGG in the presence of ISP (10 μM, 2 h), Salubrinal (5 μM, 2 h), NAC (10 mM, 2 h) and the expression of TOM20 was analyzed by confocal microscopy (a-f). U87MG cells were treated with AGG in the presence of ISP–1 and caspase 3/7 activity was determined by Caspase-Glo assay (g) and the expression was monitored as proteins by Western blot (h) and ROS through flow cytometry (i). U87MG cells were treated with AGG in presence of ISP–1 (10 μM, 2 h) and OCR was quantified (j). The data were reported as the mean ± S.D. of three independent sets of the experiment and compared with PBS control. **P-value < 0.01 was considered significant. #P-value < 0.05 and ##P-value < 0.01 were considered significant as compared to AGG treated group. Densitometry was performed on the original blots, considering the ratio of protein to actin in control cells was 1.

Tyr172 that is crucial for its interaction with LIR; the PUMA-LIR interaction is known to be crucial for PUMA-induced mitophagy [1,2] but the detailed mechanistic approach required for exploring PUMA-mediated selective autophagy is still unknown. The data generated by our study indicates that PUMA binds only to the lipidated form of LC3 (LC3-PE), as we have failed to find significant co-localization signaling between PUMA and hLC3ΔG (C-terminal Gly120 of LC3 is deleted). The interaction of PUMA with lipidated LC3 influences the induction of mitophagy in AGG treated U87MG cells. In agreement with the results of our study, C18-ceramide also binds with the lipidated form of LC3 for triggering mitophagy [30,3]. Our results show that for the promotion of mitophagy, AGG-activated PUMA binds directly to LC3 and also to ubiquitin and p62 although the latter two are not indispensable for the promotion of mitophagy. The results are supported by accumulating evidence indicating that p62 is dispensable in the case of the Parkin-mediated mitophagy [34,39] and that AGG induced mitophagy can function in a p62 dependent as well as independent manner. Interestingly, AGG induced DRP1 dependent mitophagy culminates in the induction of apoptosis in U87MG cells.

The BH3-only subset of the Bcl–2 family of proteins plays an important role in inducing apoptosis and autophagy especially mitophagy. PUMA plays an important role in stimulating apoptosis through Bax/Bak activation [16]. The previous studies have shown that PUMA-mediated activation of mitochondrial autophagy functions through the activation of the Bax pathway [17]. Interestingly, PUMA having mutant BH3 domain failed to induce autophagy whereas the deletion of the C-terminal end was not seen to affect its autophagy inducing potential. However, it showed that the C-terminal domain is necessary for directing PUMA to mitochondria rather than the N terminal fragment bearing BH3 domain for apoptosis induction [40]. In the case of NIX, it was seen that a mutation in the BH3 domain did not abrogate its potential to induce autophagy by targeting mitochondria; this indicates that the C-terminal trans-domain of this protein is necessary for both localization to mitochondria as well as for autophagy induction [41]. In the present study, we have identified LIR localized to be at 172–175 position in C-terminal domain of PUMA which interacts with LC3 to induce mitophagy. Interestingly, we also demonstrated that PUMA undergoes ubiquitination at Q151 and Y152 residues as identified previously [33] to trigger p62 dependent mitophagy. Our study concluded that the C-terminal part of PUMA is essential for mitophagy induction and that the deletion of this part is compensated by other ubiquitination sites in combination with the BH3 domain. Further studies are warranted in order to fully elucidate the details.

Ceramide, a bioactive sphingolipid, has been identified as an important molecule that can modulate both general as well as selective autophagy, especially mitophagy [42]. The recent studies have shown that ceramide interacts with LC3-II-containing autophagosomes at the mitochondrial membrane to induce mitophagy dependent cell death [30]. Ceramide signaling also regulates different cellular process such as ER stress [43], activation of BNIP3 [44] and JNK signaling [45] as a downstream signal for inducing autophagic cell death. For example, the exposure to cannabinoids leads to ceramide accumulation which in turn

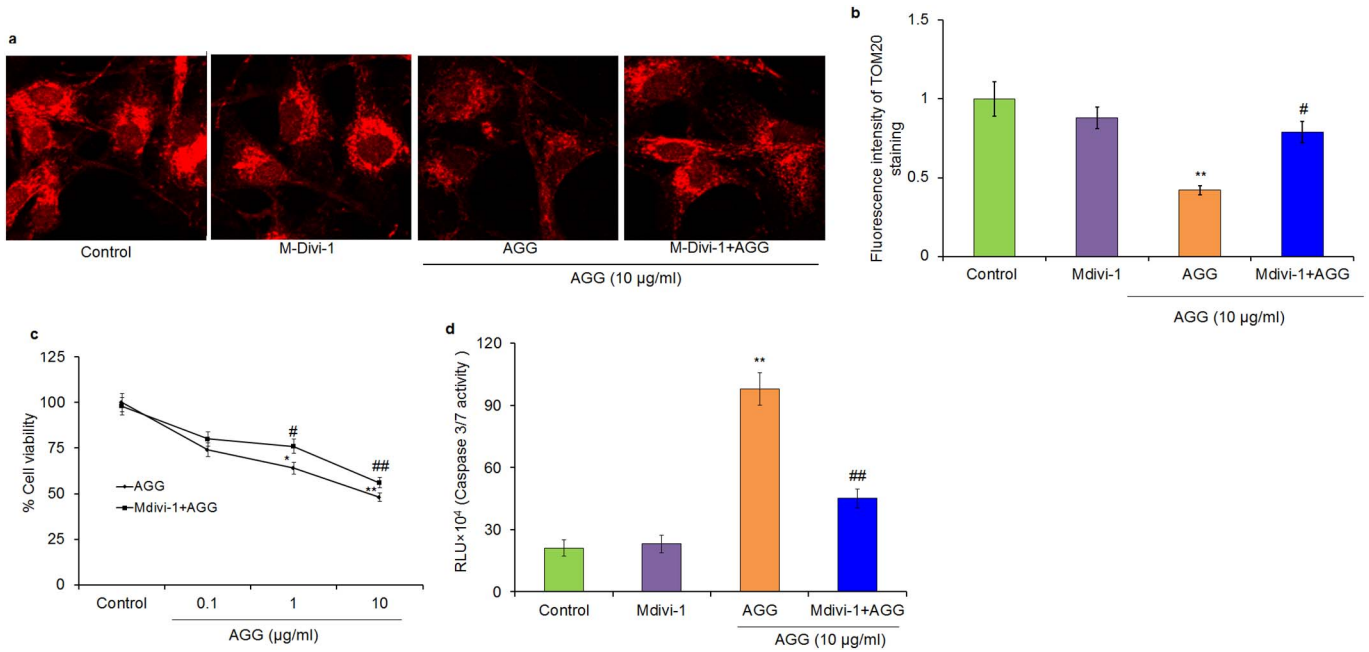

Fig. 12. AGG induced mitophagy switches to apoptosis. U87MG cells were treated with AGG in the presence of Mdivi–1 (50 μM, 3 h) and the expression of TOM20 was analyzed through confocal microscopy (a, b). U87MG cells were treated with AGG in the presence of Mdivi–1 and cell viability (c) and caspase (3/7) activity (d) were determined. The data were reported as the mean ± S.D. of three independent experiments and compared to PBS control. *P-value < 0.05, **P-value < 0.01 were considered significant. #P-value < 0.05, ##P-value < 0.01 were considered significant as compared with AGG treated group.

induces ER stress-dependent autophagic cell death in human glioma cells [43]. In accordance with this result, our study also showed that AGG induced ceramide synthesis regulated ER stress in order to promote mitophagy and that pretreatment with the inhibitor ISP–1 inhibited AGG induced mitophagy and cell death in U87MG cells supporting ceramide is a master regulator for governing AGG induced mitophagy. Although, we have identified PUMA as a mitophagy receptor during AGG associated apoptosis, the details of the underlying mechanism still remain to be elucidated. In addition, how does PUMA interact with the basic autophagy machinery at different stages of mitophagosome formation answered? Altogether, our investigation revealed two important aspects of PUMA-induced mitophagy: (a) to the best of our knowledge this is the first time it has been shown that an LIR motif may function as a crucial link between mitochondria and the autophagy machinery, and (b) an increase in the number of damaged mitochondria makes PUMA regulated mitophagy an attractive therapeutic option for the treatment of glioblastoma. In conclusion, PUMA induces mitophagy mediated cell death which has the potential to serve as an option for the treatment of cancer as well as for several mitochondrial disorders.

Conflict of interest statement

The authors have declared no conflict of interest.

Transparency document

The Transparency document associated with this article can be found, in online version.

Acknowledgments

Research support was partly provided by Department of Biotechnology [Grant Number: BT/PR7791/BRB/10/1187/2013]; the Board of Research in Nuclear Sciences (BRNS) [Number: 37(1)/14/38/2016-BRNS/37276]; Science and Engineering Research Board (SERB) [Number: EMR/2016/001246]. Research infrastructure was partly provided by Fund for Improvement of S&T infrastructure in universities & higher educational institutions (FIST) [Number: SR/FST/LSI-025/2014]. Authors were very much thankful to Lipidomics Shared Resource: Analytical Unit Medical University of South Carolina for spingolipid analysis and Supercomputer Education and Research Centre (SERC) at Indian Institute of Science (IISc) Bangalore for high performance computing facilities. PKP is obliged to DBT [BT/PR1/5090/GBD/27/309/2011] for providing fellowship. BRM is thankful to DBT BUILDER project [BT/PR-9028/INF/22/193/2013] for financial assistantship. Authors sincerely thank Sushanta Pradhan for assisting in confocal facility for this research work.

Appendix A. Supplementary data

Supplementary data to this article can be found online at https://doi.org/10.1016/j.bbamcr.2017.12.002.

References

[1] R.J. Youle, D.P. Narendra, Mechanisms of mitophagy, Nat. Rev. Mol. Cell Biol. 12 (2011) 9–14.
[2] A. Hamacher-Brady, N.R. Brady, Mitophagy programs: mechanisms and physiological implications of mitochondrial targeting by autophagy, Cell. Mol. Life Sci. 73 (2016) 775–795.
[3] G. Ashrafi, T.L. Schwarz, The pathways of mitophagy for quality control and clearance of mitochondria, Cell Death Differ. 20 (2013) 31–42.
[4] S. Mukhopadhyay, P.P. Naik, P.K. Panda, N. Sinha, D.N. Das, S.K. Bhutia, Serum starvation induces anti-apoptotic cIAP1 to promote mitophagy through ubiquitination, Biochem. Biophys. Res. Commun. 479 (2016) 940–946.
[5] R. Rojansky, M.Y. Cha, D.C. Chan, Elimination of paternal mitochondria in mouse embryos occurs through autophagic degradation dependent on PARKIN and MUL1, elife 17 (2016) 5.
[6] I. Novak, V. Kirkin, D.G. McEwan, J. Zhang, P. Wild, A. Rozenknop, V. Rogov, F. Löhr, D. Popovic, A. Occhipinti, A.S. Reichert, J. Terzic, V. Dötsch, P.A. Ney, I. Dikic, Nix is a selective autophagy receptor for mitochondrial clearance, EMBO Rep. 11 (2010) 45–51.
[7] J.Y. Chang, H.S. Yi, H.W. Kim, M. Shong, Dysregulation of mitophagy in carcinogenesisand tumor progression, Biochim. Biophys. Acta. 1858 (2017) 633–640.
[8] D. Narendra, A. Tanaka, D.F. Suen, R.J. Youle, Parkin is recruited selectively to impaired mitochondria and promotes their autophagy, J. Cell Biol. 183 (2008) 795–803.
[9] L. Liu, D. Feng, G. Chen, M. Chen, Q. Zheng, P. Song, Q. Ma, C. Zhu, R. Wang, W. Qi, L. Huang, P. Xue, B. Li, X. Wang, H. Jin, J. Wang, F. Yang, P. Liu, Y. Zhu, S. Sui,

Q. Chen, Mitochondrial outer-membrane protein FUNDC1 mediates hypoxia-induced mitophagy in mammalian cells, Nat. Cell Biol. 14 (2012) 177–185.
[10] T.E. O'Sullivan, L.R. Johnson, H.H. Kang, J.C. Sun, BNIP3- and BNIP3L-mediated mitophagy promotes the generation of natural killer cell memory, Immunity 43 (2015) 331–342.
[11] S. Geisler, K.M. Holmström, D. Skujat, F.C. Fiesel, O.C. Rothfuss, P.J. Kahle, W. Springer, PINK1/Parkin-mediated mitophagy is dependent on VDAC1 and p62/SQSTM1, Nat. Cell Biol. 12 (2010) 119–131.
[12] T. Murakawa, O. Yamaguchi, A. Hashimoto, S. Hikoso, T. Takeda, T. Oka, H. Yasui, H. Ueda, Y. Akazawa, H. Nakayama, M. Taneike, T. Misaka, S. Omiya, A.M. Shah, A. Yamamoto, K. Nishida, Y. Ohsumi, K. Okamoto, Y. Sakata, K. Otsu, Bcl-2-like protein 13 is a mammalian Atg32 homologue that mediates mitophagy and mitochondrial fragmentation, Nat. Commun. 6 (2015) 7527.
[13] Y. Wei, W.C. Chiang, R. Sumpter Jr., P. Mishra, B. Levine, Prohibitin 2 is an inner mitochondrial membrane mitophagy receptor, Cell 168 (2017) 224–238.
[14] J. Yu, L. Zhang, PUMA, a potent killer with or without p53, Oncogene 27 (2009) S71–S83.
[15] S. Mukhopadhyay, P.K. Panda, N. Sinha, D.N. Das, S.K. Bhutia, Autophagy and apoptosis: where do they meet? Apoptosis 19 (2014) 555–566.
[16] Y. Zhang, D. Xing, L. Liu, PUMA promotes Bax translocation by both directly interacting with Bax and by competitive binding to Bcl-X L during UV-induced apoptosis, Mol. Biol. Cell 20 (2009) 3077–3087.
[17] K.S. Yee, S. Wilkinson, J. James, K.M. Ryan, K.H. Vousden, PUMA-and Bax-induced autophagy contributes to apoptosis, Cell Death Differ. 16 (2009) 1135–1145.
[18] A. Bagaria, K. Surendranath, U.A. Ramagopal, S. Ramakumar, A.A. Karande, Structure-function analysis and insights into the reduced toxicity of Abrus precatorius agglutinin I in relation to abrin, J. Biol. Chem. 281 (2006) 34465–34474.
[19] S.K. Bhutia, S.K. Mallick, S. Maiti, T.K. Maiti, Antitumor and proapoptotic effect of Abrus agglutinin derived peptide in Dalton's lymphoma tumor model, Chem. Biol. Interact. 174 (2008) 11–18.
[20] S. Mukhopadhyay, P.K. Panda, D.N. Das, N. Sinha, B. Behera, T.K. Maiti, S.K. Bhutia, Abrus agglutinin suppresses human hepatocellular carcinoma in vitro and in vivo by inducing caspase-mediated cell death, Acta Pharmacol. Sin. 35 (2014) 814–824.
[21] B. Behera, K.S. Devi, D. Mishra, S. Maiti, T.K. Maiti, Biochemical analysis and antitumour effect of Abrus precatorius agglutinin derived peptides in Ehrlich's ascites and B16 melanoma mice tumour model, Environ. Toxicol. Pharmacol. 38 (2014) 288–296.
[22] S.K. Bhutia, B. Behera, D.N. Das, S. Mukhopadhyay, N. Sinha, P.K. Panda, P.P. Naik, S.K. Patra, M. Mandal, S. Sarkar, M.E. Menezes, S. Talukdar, T.K. Maiti, S.K. Das, D. Sarkar, P.B. Fisher, Abrus agglutinin is a potent anti-proliferative and anti-angiogenic agent in human breast cancer, Int. J. Cancer 139 (2016) 457–466.
[23] N. Sinha, P.K. Panda, P.P. Naik, D.N. Das, S. Mukhopadhyay, T.K. Maiti, M.K. Shanmugam, A. Chinnathambi, M.E. Zayed, S.A. Alharbi, G. Sethi, R. Agarwal, S.K. Bhutia, Abrus agglutinin promotes irreparable DNA damage by triggering ROS generation followed by ATMp73 mediated apoptosis on oral carcinoma, Mol. Carcinog. 56 (2017) 2400–2413.
[24] S.K. Bhutia, S.K. Mallick, S.M. Stevens, L. Prokai, J.K. Vishwanatha, T.K. Maiti, Induction of mitochondria-dependent apoptosis by Abrus agglutinin derived peptides in human cervical cancer cell, Toxicol. In Vitro 22 (2008) 344–351.
[25] B. Behera, D. Mishra, B. Roy, K.S. Devi, R. Narayan, J. Das, S.K. Ghosh, T.K. Maiti, Abrus precatorius agglutinin-derived peptides induce ROS-dependent mitochondrial apoptosis through JNK and Akt/P38/P53 pathways in HeLa cells, Chem. Biol. Interact. 222 (2014) 97–105.
[26] P.K. Panda, B. Behera, B.R. Meher, D.N. Das, S. Mukhopadhyay, N. Sinha, P.P. Naik, B. Roy, J. Das, S. Paul, T.K. Maiti, R. Agarwal, S.K. Bhutia, Abrus agglutinin, a type II ribosome inactivating protein inhibits Akt/PH domain to induce endoplasmic reticulum stress mediated autophagy-dependent cell death, Mol. Carcinog. 56 (2017) 389–401.
[27] R. Hegde, T.K. Maiti, S.K. Podder, Purification and characterization of three toxins and two agglutinins from Abrus precatorius seed by using lactamyl-Sepharose affinity chromatography, Anal. Biochem. 194 (1991) 101–119.
[28] J. Yu, L. Zhang, P.M. Hwang, K.W. Kinzler, B. Vogelstein, PUMA induces the rapid apoptosis of colorectal cancer cells, Mol. Cell 7 (2001) 673–682.
[29] S.R. Comeau, D.W. Gatchell, S. Vajda, C.J. Camacho, ClusPro: a fully automated algorithm for protein-protein docking, Nucleic Acids Res. 32 (2004) W96-W9.
[30] R.D. Sentelle, C.E. Senkal, W. Jiang, S. Ponnusamy, S. Gencer, S.P. Selvam, V.K. Ramshesh, Y.K. Peterson, J.J. Lemasters, Z.M. Szulc, J. Bielawski, B. Ogretmen, Ceramide targets autophagosomes to mitochondria and induces lethal mitophagy, Nat. Chem. Biol. 8 (2012) 831–838.
[31] G.M. Cereghetti, A. Stangherlin, O. Martins de Brito, C.R. Chang, C. Blackstone, P. Bernardi, L. Scorrano, Dephosphorylation by calcineurin regulates translocation of Drp1 to mitochondria, Proc. Natl. Acad. Sci. U. S. A. 105 (2008) 15803–15808.
[32] F. Kanai, H. Liu, S.J. Field, H. Akbary, T. Matsuo, G.E. Brown, L.C. Cantley, M.B. Yaffe, The PX domains of p47phox and p40phox bind to lipid products of PI(3)K, Nat. Cell Biol. 3 (2001) 675–678.
[33] B. Chen, T. Coon, R. Mallampalli, SCFFBXL18 regulates apoptosis through PUMA N-terminal linear ubiquitination, Am. J. Respir. Crit. Care Med. 19 (2015) A5082.
[34] D. Narendra, L.A. Kane, D.N. Hauser, I.M. Fearnley, R.J. Youle, p62/SQSTM1 is required for Parkin-induced mitochondrial clustering but not mitophagy; VDAC1 is dispensable for both, Autophagy 6 (2010) 1090–1106.
[35] S. Galadari, A. Rahman, S. Pallichankandy, F. Thayyullathil, Tumor suppressive functions of ceramide: evidence and mechanisms, Apoptosis 20 (2015) 689–711.
[36] D.A. Kubli, Å.B. Gustafsson, Mitochondria and mitophagy: the yin and yang of cell death control, Circ. Res. 111 (2012) 1208–12021.
[37] K. Mizumura, S.M. Cloonan, K. Nakahira, A.R. Bhashyam, M. Cervo, T. Kitada, K. Glass, C.A. Owen, A. Mahmood, G.R. Washko, S. Hashimoto, S.W. Ryter, A.M. Choi, Mitophagy-dependent necroptosis contributes to the pathogenesis of COPD, J. Clin. Invest. 124 (2014) 3987–4003.
[38] M. Villanueva-Paz, M.D. Cordero, A.D. Pavón, B.C. Vega, D. Cotán, M. De la Mata, M. Oropesa-Ávila, E. Alcocer-Gomez, I. de Lavera, J. Garrido-Maraver, J. Carrascosa, A.P. Zaderenko, J. Muntané, M. de Miguel, J.A. Sánchez-Alcázar, Amitriptyline induces mitophagy that precedes apoptosis in human HepG2 cells, Genes Cancer 7 (2016) 260–277.
[39] K. Okatsu, K. Saisho, M. Shimanuki, K. Nakada, H. Shitara, Y.S. Sou, M. Kimura, S. Sato, N. Hattori, M. Komatsu, K. Tanaka, N. Matsuda, p62/SQSTM1 cooperates with Parkin for perinuclear clustering of depolarized mitochondria, Genes Cells 15 (2010) 887–900.
[40] G. Ambroise, A. Portier, N. Roders, D. Arnoult, A. Vazquez, Subcellular localization of PUMA regulates its pro-apoptotic activity in Burkitt's lymphoma B cells, Oncotarget 6 (2015) 38181–38194.
[41] W.X. Ding, H.M. Ni, M. Li, Y. Liao, X. Chen, D.B. Stolz, G.W. Dorn 2nd, X.M. Yin, Nix is critical to two distinct phases of mitophagy, reactive oxygen species-mediated autophagy induction and Parkin-ubiquitin-p62-mediated mitochondrial priming, J. Biol. Chem. 285 (2010) 27879–27890.
[42] M. Dany, B. Ogretmen, Ceramide induced mitophagy and tumor suppression, Biochim. Biophys. Acta 21853 (2015) 2834–2845.
[43] M. Salazar, A. Carracedo, I.J. Salanueva, S. Hernández-Tiedra, M. Lorente, A. Egia, P. Vázquez, C. Blázquez, S. Torres, S. García, J. Nowak, G.M. Fimia, M. Piacentini, F. Cecconi, P.P. Pandolfi, L. González-Feria, J.L. Iovanna, M. Guzmán, P. Boya, G. Velasco, Cannabinoid action induces autophagy-mediated cell death through stimulation of ER stress in human glioma cells, J. Clin. Invest. 119 (2009) 1359–1372.
[44] S. Daido, T. Kanzawa, A. Yamamoto, H. Takeuchi, Y. Kondo, S. Kondo, Pivotal role of the cell death factor BNIP3 in ceramide-induced autophagic cell death in malignant glioma cells, Cancer Res. 64 (2004) 4286–4293.
[45] D.D. Li, L.L. Wang, R. Deng, J. Tang, Y. Shen, J.F. Guo, Y. Wang, L.P. Xia, G.K. Feng, Q.Q. Liu, W.L. Huang, Y.X. Zeng, X.F. Zhu, The pivotal role of c-Jun NH2-terminal kinase-mediated Beclin 1 expression during anticancer agents-induced autophagy in cancer cells, Oncogene 28 (2009) 886–898.